https://doi.org/10.5194/gchron-2020-31
Preprint. Discussion started: 20 October 2020

GEOCHRONOLOGY Discussions Open Access EGU

Confined fission track revelation in apatite: how it works and why it matters

Richard A. Ketcham[1], and Murat T. Tamer[1]

[1]Department of Geological Sciences, Jackson School of Geoscience, University of Texas, Austin, TX 78712, USA

Correspondence to: Richard A. Ketcham (ketcham@jsg.utexas.edu)

Abstract. We present a new model for the etching and revelation of confined fission tracks in apatite, based on step etching measurements that demonstrate variable along-track etching velocity, $v_T(x)$. We define two end-member model forms: Constant-core, with a central zone of constant etching rate that then falls off toward track tips; and Linear, in which etching rates fall linearly from the midpoint to the tips. Based on these, we construct a characterization of confined track revelation that encompasses all of the relevant processes, including penetration and thickening of semi-tracks from the polished grain surface, intersection of confined tracks, and analyst selection of which tracks to measure and which to bypass. Both model forms are able to fit step-etching data from five sets of paired experiments of fossil tracks and unannealed and annealed induced tracks, supporting the correctness of our approach and providing a series of insights into the theory and practice of fission-track thermochronology. Etching rates for annealed induced tracks are much faster than those for unannealed induced and spontaneous tracks, impacting the relative efficiency of both confined track length and density measurements, and suggesting that high-temperature laboratory annealing may induce a transformation in track cores that does not occur at geological conditions of partial annealing. The model quantifies how variation in analyst selection criteria, summarized as the ratio of along-track to bulk etching velocity at the track tip (v_T/v_B), likely plays a first-order role in the reproducibility of confined length measurements. It also shows that a large proportion of tracks that are intersected are not measured, indicating that length biasing is an insufficient statistical model for predicting the relative probability of detection of different track populations. The $v_T(x)$ model provides an approach to both optimizing etching conditions and linking track length measurements across etching protocols.

1 Introduction

Apatite fission-track confined lengths remain of great interest because of their capacity to record detailed thermal histories (Malusa and Fitzgerald, 2019; Gallagher 2012; Ketcham et al. 2018). However, our understanding of them remains incomplete in ways that are likely to be consequential for thermal history analysis. Measurements of laboratory-annealed spontaneous and induced fission tracks do not agree (Wauschkuhn et al., 2015b), leading to continuing uncertainty on the fidelity of induced tracks annealed in the laboratory as proxies for spontaneous ones annealed at geological conditions over geological time scales. Additionally, the reproducibility of length measurements among laboratories has been disappointing (Ketcham et al.,

https://doi.org/10.5194/gchron-2020-31
Preprint. Discussion started: 20 October 2020

2015;Ketcham et al., 2018). The first concern questions the theoretical basis for thermal history inversion, the second its practice.

The crucial property of fission tracks is their etching structure; the only reason we can detect and measure them at all is that they etch differently from surrounding, relatively undamaged material. The most influential aspect of this structure is the etching velocity along the track. From the earliest days of fission-track dating (e.g., Fleischer and Price, 1964), the model emerged of a fast etching velocity along the track (v_T) versus a slow etching velocity of the bulk grain (v_B, also called v_G). This contrast allows, among other things, for the calculation of a counting efficiency to quantify what proportion of surface-intersecting tracks become unobservable due to bulk etching of the polished surface obscuring shallow-dipping tracks. At the same time, it implies that v_T is constant along a track; the efficiency equation put forth by Fleischer and Price (1964) and repeated many times since (e.g., Fleischer et al., 1975;Hurford, 2019;Tagami and O'Sullivan, 2005) presumes single values for v_B and v_T.

A similar simplification is embedded in the characterization of confined track revelation by Laslett et al. (1984), in which fast etching along a track compared to bulk etching leads to track tips being hard to observe or measure reliably, but once the end of the track is reached bulk etching allows the tip to widen and become clear. A linked concept is that of maximum etchable length. Virtually all mathematical treatments of track revelation, biasing, and the relationship between confined track length and track density (Galbraith and Laslett, 1988;Galbraith et al., 1990;Laslett et al., 1984;Laslett et al., 1982;Dakowski, 1978;Jonckheere and Van Den Haute, 1999;Ketcham, 2003) presume that tracks are line segments in space, all etched to their full extents once they are intersected.

In this contribution, we demonstrate that these assumptions are incorrect, and that this shortcoming impacts AFT thermochronology in multiple ways, from reproducibility of confined track length measurements to the efficiency of track revelation that underlies age determinations. We do this by constructing the first quantitative depiction of confined track-in-track (TINT; Lal et al., 1969) revelation, incorporating their along-track etching structure as constrained by a set of recently reported step etching experiments (Tamer and Ketcham, 2020b). The model incorporates both the etching of the surface-intersecting semi-track channels and the confined tracks themselves, providing multiple insights into the nature of the confined track length distributions we measure and interpret.

2 Background

It has long been understood that etching velocity can vary along fission tracks. Fleischer and Price (1964) mention the possibility of etching slowing down toward track tips, and Fleischer et al. (1969) used diminishing along-track etching velocity to explain track geometries in track-recording plastics. Jonckheere et al. (2007) reported evidence for diminishing etching velocity toward track tips in apatite. More recent work has documented enhanced but continuously diminishing etching velocity in the region along tracks beyond where most current etching protocols reach (Jonckheere et al., 2017).

https://doi.org/10.5194/gchron-2020-31
Preprint. Discussion started: 20 October 2020

Recent step-etching experiments (Tamer and Ketcham, 2020b) demonstrate that variations in etching rates extend well into the interiors of tracks, and suggest that etching velocity should be treated as a continuous function, $v_T(x)$, where x is along-track distance, rather than a single value $v_T >> v_B$. Moreover, preliminary analysis of these data suggests that spontaneous tracks in Durango apatite have a significantly different etching structure than induced tracks lightly annealed to have a similar mean length.

Converting step-etching measurements into quantitative estimates of $v_T(x)$ is challenging, however, because track revelation is a complex process. First, surface-intersecting semi-tracks must etch into the solid crystal. As they penetrate they also widen, and this widening is the process by which confined tracks are encountered and etched (Galbraith et al., 1990;Jonckheere et al., 2007); the latent tracks themselves have a maximum diameter of about 9 nm (Li et al., 2010;Paul and Fitzgerald, 1992), and thus only intersect when track density is extremely high (Ketcham et al., 2013). A confined track may be impinged by an expanding semi-track anywhere along its length, and its revelation rate will be a function of the etching structure in both directions from that point. Finally, to be measured a confined track must be etched sufficiently to be observed, the criteria for which will differ depending on the situation. For routine AFT analysis, where the analyst evaluates whether a track is sufficiently etched, the ends of the tracks need to be clearly visible, although this evaluation is analyst-specific. For measuring tracks in early steps of step-etching experiments, the criterion is simply that a track and its tips be visible enough to make a reasonable measurement.

3 Data

The data analyzed in this study (Table 1) are confined track lengths from a series of step-etch experiments in Durango apatite in which tracks were individually followed through each etching step (Tamer and Ketcham, 2020b). Step etching data of this sort, enabled by automated image capture measurement systems (Gleadow et al., 2009), provide much clearer information on track etching than traditional step-etch experiments in which tracks are randomly selected after each etching step (Aslanian et al., in press;Jonckheere et al., 2017). We also use one single-etch-step measurement of spontaneous track lengths in Durango apatite from Tamer and Ketcham (2020a) to compare to step-etching results.

The data consist of six step-etching experiments with varying step timings and degrees of annealing, and three "etch-anneal-etch" experiments in which apatites were annealed after an initial etching step and then re-etched to obtain a robust estimate of the average bulk etching rate (v_B) at track tips of 0.022±0.004 µm/s/tip. There was no clear indication of v_B varying with track orientation (Tamer and Ketcham, 2020b). We have added to these data new measurements of the intersection points between the confined tracks and impinging semi-tracks, with the goal of evaluating model predictions for where TINT intersections occur. These measurements were made using the "cross section" tool in FastTracks software (v3), measuring the distance from each intersection to the uppermost tip of the confined track, and then converting that to true distance using track dip. In cases where it was difficult to determine if an intersection truly occurred due to interfering features, we conservatively included it.

https://doi.org/10.5194/gchron-2020-31
Preprint. Discussion started: 20 October 2020

4 The Model

4.1 Etching structure

Two simple end-member possibilities for etching velocity structure are considered (Figure 1), "Constant-core" and "Linear." Both are encompassed in Equation 1:

$$v_T(x) = \begin{cases} v_{T_{max}} & x_{T_1} \le x \le x_{T_2} \quad (1a) \\ v_{Tmax} - A\left|x - x_{T_1 \, or \, T_2}\right|;\ A = \left|\frac{\Delta v_{T_{max}-B}}{\Delta x_{T_{max}-B}}\right| & x_{B_1} \le x < x_{T_1};\ x_{T_2} < x \le x_{B_2} \quad (1b) \\ v_B & x < x_{B_1};\ x_{B_2} < x \quad (1c) \end{cases}$$

The latent track is defined by a set of etching rates along *x*, with the starting point for etching, or point where the impinging etchant pathway intersects the latent track, denoted as x_{int}. In the Constant-core model, the track middle has a constant etching rate v_{Tmax} over length Δx_{Tmax}, beyond which etching rate falls at linear rate *A* over distance $\Delta x_{T_{max}-B}$ until it drops by $\Delta v_{T_{max}-B}$ to v_B. Defining our coordinate system such that the track extends in the positive direction from one tip at *x*=0, we define coordinates x_{B_1} and x_{B_2} to be the track tips, beyond which etching occurs at the bulk rate; and x_{T_1} and x_{T_2} demarking the central zone of maximum track etch rate. The Linear model is simply the special case where Δx_{Tmax} is zero. We define the latent track length L_{lat} as the entire zone of enhanced etching velocity:

$$L_{lat} = \Delta x_{Tmax} + 2\Delta x_{T_{max}-B} \quad (2)$$

Only simple models justifiable at this point because our data consist of a very limited number of experiments. The Linear model is simpler, but the Constant-core model includes the simplest possibility of constant etch rate for the entire track if Δx_{Tmax} equals the entire latent track length. These models may be considered end-members of a more complex model in which reduction in etch rate slowly accelerates as the track tips are approached. For this initial effort, we neglect length and etching anisotropy, as well as other complexities such as the likely asymmetric nature of true tracks due to the asymmetric energies and masses of the fission particles.

To convert the etching structure to the time required to etch out to a certain length, we integrate Equation (1). For simplicity, we etch in the positive direction toward x_{B_2}, and denote the half-length toward that point as L_2. Etching of the grain mount commences at time *t*=0, and the confined track starts to etch at a later time t_s, to account for the time necessary to propagate and widen the impinging track sufficiently to intersect the latent confined track. There are three cases to consider depending on where x_{int} is: in the tip nearest x_{B_2}, in the constant-rate core, or in the tip nearest x_{B_1}. If x_{int} is in the constant-rate core, the second case, then the time required to etch to a half-length L_2 is:

$$t(L_2) = \begin{cases} t_s + \frac{L_2}{v_{T_{max}}} & L_2 \le x_{T_2} - x_{int} \quad (3a) \\ t_s + \frac{x_{T_2} - x_{int}}{v_{T_{max}}} + \int_{x_{T_2}}^{x_{int}+L_2} \frac{dx}{v_T(x)} & x_{T_2} - x_{int} < L_2 \le x_{B_2} - x_{int} \quad (3b) \end{cases}$$

https://doi.org/10.5194/gchron-2020-31
Preprint. Discussion started: 20 October 2020

$$t_s + \frac{x_{T_2} - x_{int}}{v_{T_{max}}} + \int_{x_{T_2}}^{x_{B2}} \frac{dx}{v_T(x)} + \frac{L_2 - (x_{B2} - x_{int})}{v_B} \qquad x_{B_2} - x_{int} < L_2 \qquad (3c)$$

After integrating, the solution becomes:

$$t_s + \frac{L_2}{v_{T_{max}}} \qquad L_2 \le x_{T_2} - x_{int} \qquad (4a)$$

$$t(L_2) = \quad t_s + \frac{x_{T_2} - x_{int}}{v_{T_{max}}} - \frac{1}{A}\ln\left(1 + \frac{x_{T_2} - (x_{int} + L_2)}{\frac{v_{T_{max}}}{A}}\right) \qquad x_{T_2} - x_{int} < L_2 \le x_{B_2} - x_{int} \qquad (4b)$$

$$t_s + \frac{x_{T_2} - x_{int}}{v_{T_{max}}} - \frac{1}{A}\ln\frac{v_B}{v_{T_{max}}} + \frac{L_2 - \left(x_{B_2} - x_{int}\right)}{v_B} \qquad x_{B_2} - x_{int} < L_2 \qquad (4c)$$

Solving these equations for half-length as a function of etching time then gives:

$$0 \qquad t \le t_s \qquad (5a)$$

$$v_{T_{max}}(t - t_s) \qquad t_s < t \le t_s + \frac{x_{T_2} - x_{int}}{v_{T_{max}}} \qquad (5b)$$

$$L_2(t) = \quad x_{T_2} - x_{int} + \frac{v_{T_{max}}}{A}\left[1 - e^{-A\left(t - t_s - \frac{x_{T_2} - x_{int}}{v_{T_{max}}}\right)}\right] \qquad t_s + \frac{x_{T_2} - x_{int}}{v_{T_{max}}} < t \le t_s + \frac{x_{T_2} - x_{int}}{v_{T_{max}}} - \frac{1}{A}ln\left(\frac{v_B}{v_{T_{max}}}\right) \qquad (5c)$$

$$x_{B_2} - x_{int} + v_B\left[t - t_s - \frac{x_{T_2} - x_{int}}{v_{T_{max}}} + \frac{1}{A}ln\left(\frac{v_B}{v_{T_{max}}}\right)\right] \qquad t_s + \frac{x_{T_2} - x_{int}}{v_{T_{max}}} - \frac{1}{A}ln\left(\frac{v_B}{v_{T_{max}}}\right) < t \qquad (5d)$$

Solutions to the other two cases are provided in the Appendix. L_1 is calculated using the same set of equations by changing the value of x_{int} to $L_{lat} - x_{int}$.

Figure 2 illustrates the implied growth curves of tracks in each case, using Constant-core model rates for unannealed induced tracks calculated later in this paper (Table 2). Lengthening is mostly nonlinear, accelerating and decelerating depending on local etching structure and asymptotically approaching the bulk etch rate toward track tips. An immediately interesting outgrowth of this model is that etched track length after a given amount of time varies depending on where the track is intersected by the etchant pathway. Figure 2C,D shows the development of total track length with time etching depending on impingement point. Impinging the track center is most efficient, as equal etching can occur in both directions. If the impingement is toward one end then the result is a shorter track, as in one direction the etchant quickly reaches the near tip, while in the other it must first make its way through a slower region to get to the faster etching core on its way to another slow-etching region toward the far tip. Variation in impingement point alone is likely responsible for some component of the observed variation in track lengths.

4.2 Semi-track penetration and confined track revelation

For internal surfaces (i.e. grains mounted and polished to remove ~10 µm or more of material), tracks will originate from fission events both above and below the polished surface, and will cross the polished surface at all possible angles. Although track angles are uniformly distributed, their crossings are subject to two biases. First, the relative probability of a track of

https://doi.org/10.5194/gchron-2020-31
Preprint. Discussion started: 20 October 2020

latent length or half-length L crossing the surface plane will depend on track dip δ as L sin δ. Second, the relative abundance of tracks at dip δ will vary as cos δ, by analogy of the area between latitude lines on a globe. Thus, the probability of a semi-track occurring will be proportional to L sin δ cos δ. The x_{int} point at which the track intersects the polished surface is evenly distributed along its length. The semi-track penetration calculation thus consists of randomizing some number (typically 10^5) lengths, dips, and x_{int} points, and then using the etching model to trace each semi-track's penetration into the grain surface.

We also consider the case of implanted ion tracks, whether from ^{252}Cf or a particle accelerator. Here the surface intersection angles and x_{int} points are not random, but constant. As ^{252}Cf irradiation was used for some of our data, we use a mean ^{252}Cf semi-track length of 5.9 µm with standard deviation of 1.4 µm, based on unpublished measurements at the University of Texas. We also assume a dip of 75°; Jonckheere et al. (2007) point out that, to maximize etching efficiency, ion tracks should not be normal to the polished surface.

Confined track revelation requires that, once the semi-track has reached a given depth, it then begins to etch outward into the bulk crystal at that depth, at the bulk etching rate, even as it continues to propagate downward. The probability of a semi-track encountering a confined track at a given depth is proportional to the radius of this etched zone at that depth, increasing as the track widens. Revelation is actually anisotropic based on the shape of the etch figures (Galbraith et al., 1990;Ketcham, 2003) or internal crystallographic planes (Jonckheere et al., 2019), but we omit this consideration for our simplified initial model.

Figure 3 shows examples of penetration and revelation rate. For randomly oriented tracks on an internal surface (Fig. 3A, B), net penetration and revelation develop relatively slowly, as the majority of tracks are at a relatively low angle to the grain surface. It is also noteworthy that penetration is limited, and that ~10% of tracks reach a depth of only 1 µm or less. Although the ^{252}Cf tracks are shorter, as they reflect only one fission particle, penetration and revelation are relatively fast because of their consistent and efficient orientation (Fig. 3C, D).

4.3 Confined track intersection

The data represented in Figure 3B or 3D are used to calculate a cumulative distribution function (CDF) for intersecting possible confined latent tracks as a function of time and depth. We generate some number of intersecting tracks with a distribution of dip angles ranging from 0 to δ_{max}, weighted as cos δ. For this study we use a δ_{max} of 25°, near to the maximum measured in the Tamer and Ketcham (2020b) data set. We also randomize the impingement point (x_{int}) along each latent track, using a uniform distribution but excluding regions near the track ends, which can obscure the etched tip and make it unmeasurable. For the present work we define this exclusion region to be within 2 µm of each latent track tip.

Based on the length, dip and impingement point, some of the tracks generated intersect the grain surface, or in other words are semi-tracks themselves. We thus cull all tracks with an upper endpoint 0.5 µm or less below the surface; the buffer region accounts for bulk etching down from the original surface and vertical widening of the track.

Figure 4 shows an example model of 10^7 track intersections generated over 20 s of etching. The contour plot of all intersections (Fig. 4A) shows that tracks are more likely to be intersected near the surface, and more likely to be intersected later in the etch

https://doi.org/10.5194/gchron-2020-31
Preprint. Discussion started: 20 October 2020

than earlier. This result is a direct outgrowth of the revelation rate calculation (Fig. 3B); as time goes on, more semi-tracks are penetrating deeper and getting wider, increasing the probability of intersecting other tracks at depth. Only a fraction of tracks intersected are confined tracks, however. Figure 4B shows that only about half of the generated interior tracks remain after surface-intersecting tracks are excluded. Note that this proportion should not be taken as an absolute, as it is influenced by the range of dips included in the calculation.

4.4 Confined track selection

Once the impingement time and along-track location (t_s and x_{int}) are generated for a confined track, its etched length through time is calculated. Because track intersection occurs continuously, etched lengths will range from negligibly short up to the longest track etched. However, not all of them will be selected for measurement. For normal AFT analysis, the analyst aims to measure only tracks that are "fully etched" or, as proposed by Tamer and Ketcham (2020b), "sufficiently etched" according to the analyst's judgement. Making this determination is a matter of training and experience, however, and it is to a significant degree arbitrary. It is based primarily on the appearance of the track tips, which will develop as a function etching velocity along the track, or $v_T(x)$.

For convenience, we define the tip etching state in terms of the ratio $v_T(x)/v_B$ (or, more briefly, v_T/v_B) at the etched tip, though the actual tip state will also depend somewhat on the slope of $v_T(x)$ leading up to the tip. We further propose that, to first order, each analyst has a characteristic v_T/v_B for tracks that they decide are sufficiently versus insufficiently etched. In our model each track is evaluated based on the tip with the largest v_T/v_B value.

Figure 5 shows a rough calculation of the evolution of a track tip through a series of etching times, using $v_T(x)$ for along-track etching and v_B for etching perpendicular to the track. This calculation is simplified compared to recent work that endeavors to incorporate the detailed etching structure caused by internal crystal lattice planes and the angle of the track (Aslanian et al., in press;Jonckheere et al., 2019), but it is a reasonable depiction of a track at ~45° to the **c**-axis. As $v_T(x)$ falls along the track, the tip widens and becomes more distinct far before the true end of the track is reached; when v_T/v_B finally falls to a value of 1.0, the track is bulbous by normal AFT analysis standards. Most, perhaps all, analysts would judge the track as sufficiently distinct to measure at some earlier stage. Given the large length change with even subtle changes in track tip shape, more than 2 µm as v_T/v_B goes from 11 to 1, it is evident that analyst judgement in tip evaluation can be a first-order factor in explaining inter-analyst variation in track measurement.

For step etching experiments with first steps shorter than 20 s, precise location of the tip is not a prerequisite for track selection, which is instead a matter of simple visibility. In the earliest stages of etching, tracks will be too thin to be observable in visible light. As they grow, they become more efficient at reflecting light, making them more detectable. However, when this occurs in the context of practical fission track analysis is unclear.

Lacking a physical basis for determining when etched tracks begin to become visible, we examined the shortest tracks measured during the initial etching steps, and by trial and error constructed an empirical two-component operator bias function for the probability of an etched track becoming visible. Etching time must be greater than 3 s, after which track observability

https://doi.org/10.5194/gchron-2020-31
Preprint. Discussion started: 20 October 2020

the probability of selecting a track is represented as $((L - 4.5)/5.5)^3$; no tracks are observed below 4.5 µm and all tracks are observed by 10 µm, with a power-law increase in probability between those lengths. We note that this latter formulation only applies to tracks in their initial stages of etching, and not to truly short tracks that etch long enough to widen.

Both observability criteria and their outcomes are demonstrated in Figure 6. Figure 6A shows the short-first-step probability of measurement, and Fig. 6B shows the length distribution for unannealed induced tracks after 10 s (experiment SE2), and the tracks that are selected. Aside from not accounting for a few very short tracks <6 µm, the model size distribution is very similar to the measured one (Fig. 6C). Figure 6D-F shows the corresponding case standard track selection after a 20 s etch (experiment SE1). The tracks have a range of tip development (Fig. 6D), and only selecting those with $v_T/v_B \leq 12$ (Fig. 6E) results in an excellent match to the measured data (Fig 6F). The model histograms (Fig. 6B, E) also provide an indication of how many, or few, confined tracks are selected relative to how many are etched.

In addition to lengths, the model also predicts the depth and etching time distribution of selected tracks. Figure 7 shows the distribution of track lengths and etching times with depth below the surface. It's clear that most selected tracks are intersected close to the surface, as that is the area best sampled by expanding semi-tracks, and substantial time is required to sufficiently etch a track once it is intersected, which will be a function of the along-track etching structure (Fig. 7A). There is a modest decrease in mean length with depth (Fig. 7B) owing to deeper tracks on average taking longer to be intersected. Only about 2.3×10^5 tracks pass the selection criteria, 2.3% of the 10^7 generated for this model, or 5.0% of those that are confined (Fig. 3). Again, this proportion is partly a function of the range of dips permitted.

4.5 Fitting step-etching data

Fitting the experimental data consists of posing an etching structure and using it to construct first a semi-track distribution and then a distribution of etched lengths. For multi-step experiments, tracks selected after the first etching step are then allowed to lengthen through subsequent etching steps. The resulting mean track lengths are calculated, and compared with the measured mean lengths. The merit function is reduced chi-squared (χ^2_ν).

We also include the option to incorporate some innate variation in latent track length. For the modeling in this paper we chose a σ of 0.5 µm, based on the scatter of lengths after **c**-axis projection to remove anisotropy effects (Donelick et al., 1999;Ketcham, 2003). Incorporating this factor has only a minor effect on the mean length and thus fitted model parameters, but results in a better match to measured length histograms. Dispersion is modeled as a variation in latent track length, with core length proportionally reduced in the common-core models, while $v_{T,max}$ was kept constant. Because shorter tracks etch to their tips more quickly and are thus more likely to be selected, including this scatter lowers predicted mean lengths slightly, with a more severe effect at higher v_T/v_B values: by ~0.2 µm at $v_T/v_B = 4$, down to less than 0.1 µm at $v_T/v_B = 12$.

The step etch experiments only consist of 3-5 steps, making it difficult to meaningfully constrain models with 2-3 variables defining etching structure, in addition to biasing factors. To increase the amount of data, we paired data sets based on the same or equivalent tracks. Thus, we simultaneously fit data sets SE1 and SE2, both of which analyzed unannealed induced tracks, but with different initial etching steps. This allows the model to attempt to reproduce the effects of different selection biases

https://doi.org/10.5194/gchron-2020-31
Preprint. Discussion started: 20 October 2020

(one based on 10s of etching, one on 20s). Similarly, we co-fit SE3 with a single-step 20s measurement of unannealed fossil tracks from Tamer and Ketcham (2020a). For the annealed induced track experiments (SE4, 5, 6), we simultaneously fit the first 10-s etching step of the corresponding etch-anneal-etch experiments (EAE1, 2, 3). To minimize the effect of the biasing factors, we used the same ones for all modeling. After several trials, we settled on a v_T/v_B of 12, as well as the observer bias function and values for minimum tip depth and near-tip exclusion zone for impingement. With regard to fitting, the observer biasing criteria essentially truncate the short part of the track length distribution, while the etching structure and time define the longer part of the distribution (Fig. 6B, E). In essence, both have to fit, or compensate each other, to match the measured mean track length data.

During fitting of the unannealed induced track data (SE1 and SE2), it became apparent that one pair of data points were exerting outsized control on the result. Since the 15-20 s and 20-25 s steps for experiment SE2 feature the very similar mean length reduction and thus almost the same rate, in the context of our model forms assuming a linear rate decrease fits were forced to split this difference to the exclusion of closely fitting the rest of the data for SE1 and SE2. We thus excluded the 15-s mean length for SE2, effectively making the second etching step go from 10 s to 20 s.

Model fitting is complicated by each calculation of predicted track lengths incorporating several randomizations: semi-track orientation and surface intersection points; internal track orientations, depths, and intersection points; and which short tracks are observed. As a result, the same set of model parameters generates slightly different predictions with each model run, and there is no true minimum to converge to, making it difficult to avoid temporary local minima. We thus fitted the models using the downhill simplex method (Press et al., 1988) over multiple iterations from multiple starting points, stopping each run after testing 50 models, which by inspection was a sufficient number for the algorithm to converge toward a local minimum and no longer significantly change parameter values being attempted. For Constant-core models, the variables showed a high degree of correlation and χ^2_ν broad minima, requiring running many more simplex instances from different starting points to trace out these correlations.

The parameter sets we report are those that achieved the lowest χ^2_ν for each data set, but they are somewhat arbitrary because repeated runs using the same parameters result in a range of χ^2_ν values, and different parameter sets may be able to reach lower scores. Due to these complexities, we define confidence intervals by running 20 repetitions of the lowest-χ^2_ν parameter set for each data set, determining the mean and relative deviation of χ^2_ν. The confidence intervals include all parameter sets tested during the simplex runs with χ^2_ν values within two deviations of the mean.

5 Results

Table 2 shows the fitted model parameters and confidence intervals, along with the mean χ^2_ν values and relative deviations, and the right-hand columns of Table 1 show the model predictions. For the Constant-core model, all but the unannealed induced track data fits have χ^2_ν values below 1.0, indicating that fits are well within measurement uncertainties. For three data

https://doi.org/10.5194/gchron-2020-31
Preprint. Discussion started: 20 October 2020

sets, the Linear models fit almost or equivalently as well as the Constant-core, but for SE3 and SE5, the Constant-core fits are better. The standardized residuals for each fit to each data set (Figure 8) show that almost all experimental results were reproduced to within 2σ, and there are no indications of any systematic patterns in the misfits. A complete set of model outputs for each data set is provided in the Supplement to this paper.

Figure 9 shows the parameter fits for Constant-core models, and Figure 10 for Linear models. Constant-core models tend to support a long stretch of solutions trading off core length for maximum etching velocity that in some cases reaches to a core length of zero, the Linear model case. Constant-core model results for latent track length are relatively stable with respect to the other parameters, however, and predict ~0-0.2 shorter latent track length than Linear models, with higher divergences for longer cores. Linear model fits show a correlation between maximum etching velocity and mean latent track length for the unannealed experiments, but little to no correlation for the annealed experiments.

The starkest difference in etching structure is evident in Figure 11, showing Linear model maximum etching velocity and velocity gradient for the different experiments. Unannealed induced and fossil tracks both have slow-etching central regions, whereas all samples with laboratory annealing have fast etching rates in their centers. The fall-off in etching velocity from track centers to tips occurs at a 2.6-3x faster rate for the annealed experiments compared to the unannealed ones.

Figure 12 shows the distributions of intersection depths between semi-tracks and confined tracks, measured from the image data for the final etching step in each experiment. It also shows the mean intersection depths, which can be compared against model predictions in Table 1, and the number of intersections per track. The number of intersections per track is unusually high due to the large latent track densities, and Cf irradiation for SE3. We do not know precisely when these intersections occurred, however, and in particular whether a given semi-track intersected a still-latent part of the confined track, or one that was already etched. The predictions in Table 1 correspond to the first impingement, and we have not estimated how many additional impingements might be expected. Also shown is the spacing between captured images for each experimental data set, corrected for the apatite refractive index, which could have affected depth resolution.

6 Discussion

It is remarkable that we are able to reproduce the mean length data in each etching step of all experiments simultaneously using these simple models of etching structure, with a consistent set of assumptions about track detectability and selection. Many otherwise odd-appearing features of the data turn out to be natural outgrowths of how experimental protocols interact with diminishing etching velocity. For example, our results verify that the 0.4 µm longer mean track length after 20 seconds of etching in experiment SE2 versus SE1, and SE3 versus TK20, is a direct result of the SE2 and SE3 tracks being selected after 10 seconds, leading to the measured tracks being etched an average of 2.2-2.4 s longer. Similarly, the unexpected observation that annealed tracks (EAE1, 2, 3) are longer than unannealed ones (SE2, 3) after 10 seconds of etching is readily explainable by a change in etching rates that is consistent with measurements after longer initial etching steps. We take these

https://doi.org/10.5194/gchron-2020-31
Preprint. Discussion started: 20 October 2020

successes as an indication of the overall correctness of our characterization of confined track etching. Our results also point to the potential for ascertaining the true latent track length; estimates are within 0.2 µm of each other for the two models.

One aspect of the data not reproduced well are the impingement depths (Fig. 12). As mentioned previously, a number of experimental factors and unavoidable ambiguities complicate the comparison, the largest being that we do not know which impingement happened first for each track. A more significant question is whether multiple impingements to the same tracks caused faster etching, leading to inappropriate etching velocity determinations. While this is a concern, we do not believe that our etching rates are significantly affected by multiple impingements. Our slowest-etching sample, SE3, has about that same number of impingements per track as the EAE experiments that establish the fast early etching rates for the annealed experiments, and more impingements per track than the faster-etching SE1 and SE2. For an additional impingement to accelerate track revelation substantially, it would probably need to intersect an as-yet-unetched part of the track. Thus, to have a substantial effect on etch rates, follow-on impingements must happen within a few seconds of and at a distance from the first one, whereas impingements with no effect can occur at any time, anywhere along the track. Impingements also become more likely when both the semi-track and confined track are widening, in essence growing to meet each other. We finally note that our impingement numbers are probably high, as we counted all likely impingements, but it can be difficult to determine whether there is a true impingement or a near miss. In sum, the most likely consequence of our high impingement numbers may be an over-estimation of the etch rates of our annealed track experiments, but not enough to change any of the broad conclusions we draw from those data.

6.1 Model form

The success of both the Constant-core and Linear model forms in fitting the data clearly indicates that etching rates start diminishing well before the tips are reached; although a constant etch rate would work for annealed sample SE5 (Fig. 9D), it is untenable for the data as a whole. However, there is considerable variability and uncertainty in the length of the core zone in the Constant-core models. We take this as an indication that neither model is a perfect rendering of the etching structure of a track. Etching rate may be linked to latent track cross section diameter, which gradually shrinks from the fission site to the tips (Li et al., 2012). The TEM data suggest the existence of an inflection point from slower to faster diameter reduction, which a linear combination of the Linear and Constant-core model would roughly approximate. However, such a model would take four parameters to define (maximum etch rate, etch rate at inflection point, width of interior zone, latent length), which is too complex for the limited amount of data we have, and thus we prefer to use only simple models at this stage. Smooth functions are of course also possible, and arguably preferable, but would also require as many or more degrees of freedom.

It is also possible that falling directly to our measured v_B is an oversimplification of the latent track tip, and that etching velocity asymptotically approaches a limiting and lower bulk value due to sporadic damage remnants, as postulated by Jonckheere et al. (2017) and Aslanian et al. (in press). We cannot rule this possibility out, but consider it likely to have at most a minor influence on practical observations, as they needed to etch for more than 40 seconds to reach inferred etching rates for Durango apatite lower than our value for v_B.

https://doi.org/10.5194/gchron-2020-31
Preprint. Discussion started: 20 October 2020

6.2 Fossil versus induced tracks

Fossil and unannealed induced tracks have slow core etching rates, while all annealed induced tracks have far higher rates. This implies that the high temperatures used for laboratory annealing experiments may reorganize the atoms in the track core in a way that does not occur during geological low-temperature annealing. This may be responsible for some component of the mismatch in annealing fossil versus induced tracks in laboratory experiments (Wauschkuhn et al., 2015a), although we do not yet have data to gauge whether high-temperature annealing of fossil tracks has the same effect as on induced ones. Also, since the annealing that affects lengths takes place at the tips, the significance of what takes place in the core region is unclear. Nevertheless, the implied mismatch between fossil and annealed induced tracks may be a concern.

6.3 The line segment model and length bias

Mathematical treatments of fission-track lengths are all based on a line segment model (Laslett et al., 1982;Parker and Cowan, 1976), which posits latent tracks as line segments within a volume that are detected and become fully etched when intersected. One outgrowth of the line segment model is length biasing; the probability of intersecting and thus detecting and measuring a latent track is proportional to its length. This study shows this to be an oversimplification. Many more tracks are intersected than measured (Fig. 6), because of the significant time required to etch. The controlling parameter on detectability then becomes how quickly they become sufficiently etched to be accepted by the analyst, which in turn depends on length, etching velocity structure, and analyst criteria. Figure 13 shows example model prediction of tracks based on SE1 (unannealed) and SE4 (most highly annealed) induced tracks, both revealed using Cf semi-tracks to give a common baseline. Only 6.5% of the confined unannealed tracks end up being selected, due to slow etching requiring at least 9 s and on average 13 s for tips to be sufficiently revealed (assuming v_T/v_B = 12). Because the annealed tracks etch more quickly and don't have as far to etch, requiring as little as 4 seconds and averaging 8, 42% of confined tracks intersected are sufficiently etched to be selected. If we take into account the 2-µm exclusion zones at each track tip, the line segment model states that the annealed tracks are only 65% as likely to be intersected as the unannealed ones. This remains a source of bias, but even after incorporating this intersection probability, the annealed confined tracks are over four times more likely to be selected for measurement than unannealed ones.

This is an extreme example, as we have no reason yet to expect that fossil tracks with varying levels of annealing have this degree of etching rate variation, but it demonstrates that etching properties can be far more influential than length biasing in determining the relative probability of track measurement. Length biasing is a central assumption embedded into track length modeling (Green et al., 1989;Ketcham, 2005;Willett, 1997), as it determines how to construct a combined track length distribution from individual populations of tracks generated throughout a geologic history. A substantial change in inter-population biasing will alter the shape of time-temperature paths by changing the proportion of time spent at different temperatures required to generate a given observed track length distribution. A thorough re-evaluation of this biasing based on measurements of fossil track etching structure is thus a necessity for setting such modeling on a firmer foundation.

https://doi.org/10.5194/gchron-2020-31
Preprint. Discussion started: 20 October 2020

6.4 Sources of analyst variability

Our model illuminates how the measured length distribution for a single population of tracks is controlled on the long side by the maximum extent of etching, and on the short side by the analyst's selection criteria. This idea leads to a very compelling explanation for the observed variability in inter-laboratory studies: different judgement of track tips. In their international, inter-laboratory exercise, Ketcham et al. (2015) reported variation in measured track length for unannealed induced tracks in Durango apatite across all levels of analyst experience, and without any obvious linkage to specific etching protocol (Fig. 14). Table 3 and the histograms on the bottom of Figure 14 shows the corresponding model predictions, varying only v_T/v_B. Virtually the entire range of the data can be explained by this one parameter; 72% of results lie between the predictions for 16 and 4, and 35% between 12 and 8. The median track length measurement was 15.9 µm, which corresponds to a v_T/v_B value of 9 (or 10 if no scatter in latent length is included).

As v_T/v_B rises, the proportion of accepted tracks increases, and the mean track length falls; essentially, relaxing tip selection criteria makes it easier to measure a large number tracks. Conversely, using restrictive criteria can strongly reduce the number of tracks measured, but also reduces scatter, making the information in the individual tracks lengths less ambiguous. Figure 15A shows the observed relationship of mean length to standard deviation with anisotropy effects removed for the Ketcham et al. (2015) exercise. The increase in standard deviation predicted by the model matches the data quite well; a slightly better match could be forced by increasing the baseline scatter of latent lengths in the $v_T(x)$ model above $\sigma = 0.5$ µm, but that would presume that all scatter was due to selection criteria, which we do not believe is necessarily the case. The model prediction, and the data, also indicate that scatter does not start increasing until the mean length falls below 16 µm, or a v_T/v_B value of about 8. Figure 15B and Table 3 show that the number of tracks that meet a given v_T/v_B standard begins to rapidly rise as the standard is relaxed; for example, a v_T/v_B standard of 12 provides 2.5x as many tracks as a v_T/v_B of 8, and 33x as many as a v_T/v_B of 4.

Because having a high number of confined tracks is better for thermal history modeling, there is a practical incentive to adopt criteria that will provide reasonable numbers of tracks for a reasonable amount of effort. This may create a tension between having demanding tip criteria to ensure tracks are "fully etched," versus accepting a lower level of etching that provides more tracks. One way to ameliorate this tension is with ^{252}Cf or ion track irradiation, which makes it easier to achieve high numbers while retaining very demanding tip criteria. However, we note that even the longest measurements reported by Ketcham et al. (2015), likely reflecting the most rigid criteria, still do not reach the mean latent track length of 17 µm indicated by our data and model.

Another option is to maintain very consistent criteria, even at a diminished level of tip etching, which effectively fixes the shorter part of the track length distribution in place. The considerable variation observed among even experienced analysts in the Ketcham et al. (2015) exercise likely represents this occurring, but at differing degrees of etching, in various lab groups. The model introduced here potentially provides the capability to evaluate the trade-offs between efficiency and dispersion.

https://doi.org/10.5194/gchron-2020-31
Preprint. Discussion started: 20 October 2020

However, to do so, more information is required to better document effects of track angle, apatite solubility, and etching rates of fossil tracks.

Yet another avenue to improvement may be to utilize other measurements that can be made on tracks, such as tip shape (through image analysis) or track thickness (Aslanian et al., in press), to evaluate degree of etching, and construct a suitable compensation factor. Indeed, ultimately it may be possible to use machine learning to train an algorithm to evaluate degree of track etching. Again, many more measurements will be required, and the context provided by an etching model will be important to any such effort.

Analyst variability in tip evaluation may also underlie the different trends seen in length versus **c**-axis angle (ϕ) distributions among analysts (Ketcham et al., 2015;Ketcham et al., 2007b). Because etched track morphology changes with **c**-axis angle, and because tip visibility diminishes in low-angle and very high-angle tracks, different choices made by analysts on which of these tracks to accept versus reject may be responsible for the different observed trends in L_c vs. L_a (the **c**-axis and **a**-axis intercepts for ellipses fit to length versus ϕ). Moreover, changes in etching structure and thus tip revelation between annealed induced and fossil tracks could shift the appropriate **c**-axis projection between these track types.

What is the best way to overcome analyst variability? One avenue may be improved training and community consultation so all agree on what a sufficiently etched tip is. Such a prescription may be tricky, however, as tip appearance depends on multiple factors, including mount preparation, polishing, and cleaning technique, microscope optics, and captured image quality, which will vary over the community and can be expected to slowly improve over time. An alternative may be to use measurements of standards to determine an analyst's v_T/v_B (or some other indicator quantifying selection criteria), and use that as a more informative renormalization parameter than simply the unannealed induced track length. Whereas length normalization consists of simply dividing mean lengths by an initial length, utilizing v_T/v_B may allow us to account for how different tip evaluation criteria affect measurements differently at various levels of annealing.

There is also the question of whether and how etching procedure matters. Etchant strength affects etch figure shape, and must affect both along-track and bulk etching rates, perhaps by different factors for each. We note that the overall schema that we are proposing contradicts some aspects of our own recent interpretation of why two major etching protocols (5.5 M HNO_3, 21°C, 20 s vs. 5.0 M HNO_3, 20 °C, 20 s) produced different results in a detailed comparison by two analysts (Tamer et al., 2019). We interpreted this to reflect that the weaker etchant and lower temperature resulted in more under-etched tracks, leading to shorter mean track lengths. However, the $v_T(x)$ model makes clear that under-etched tracks are always present; it is merely a question of whether they are selected. Whether more under-etched tracks were chosen because better-etched tracks were more uncommon, or because the different etchant subtly affected their appearance, or because of some other factor, we cannot establish at this time. It may be reasonable to infer, however, that maintaining consistent selection criteria is more important than consistent etching procedures for making reproducible measurements.

https://doi.org/10.5194/gchron-2020-31
Preprint. Discussion started: 20 October 2020

6.5 Normalization and annealing models

Ideally, divergences in analyst measurements can be overcome by normalizing them to some standard, usually the measurements that underlie the annealing model used to interpret their data (Barbarand et al., 2003;Carlson et al., 1999). Typically, this normalization consists of dividing by a determination of initial track length (L_0; unannealed induced tracks) by the analyst, employing the same procedures used for unknowns (e.g., Green et al., 1986). The results of this study, however, suggest that this approach may be oversimplified and in need of improvement. Table 4 contains model predictions for three track types across three v_T/v_B selection criteria. The predicted mean track length for unannealed induced tracks (SE1) ranges from 15.6 to 16.3 µm after 20 s of etching as selection criteria grow more strict. Using these values to normalize the unannealed spontaneous track measurements works very well (L/L_0 = 0.912-0.915). However, due to their faster etching rates, the predicted lengths of annealed sample SE4 are much more stable (12.4-12.5 µm), and the normalization actually destabilizes them (L/L_0 = 0.766-0.790). There is some indication of this phenomenon in the sample from the Ketcham et al. (2015) inter-laboratory study with the most similar level of annealing, DUR-1. Agreement in raw length measurements was arguably best for that sample among the four in that study, and normalizing by initial length alone actually increased the scatter among several laboratories (compare Fig. 3B and 7B in Ketcham et al., 2015). Convergence was maximized only after also normalizing for track angle using **c**-axis projection (and omitting results for which no angle measurements were provided).

It may be that etching rates remain low in annealed fossil tracks, reducing this divergence in behavior and improving the performance of regular normalization for geological investigations. However, this remains to be established via measurements. Even so, an improvement in cross-normalization of measurements of annealed induced tracks would be valuable, as a means of increasing the inter-compatibility of length measurements across different experimental annealing studies. Mostly minor but occasionally consequential differences in annealing temperatures predicted by the Ketcham et al. (1999) annealing model based on Carlson et al. (1999) measurements, versus the Ketcham et al. (2007a) model which combined these with the Barbarand et al. (2003) results, may be due to oversimplified normalization.

The clearer picture of track structure provided by the $v_T(x)$ model may improve our understanding of annealing and annealing models in other ways as well. Our derived true mean latent track lengths in Durango apatite (~17.0 µm induced and ~15.5 µm fossil) are significantly longer than measurements obtained with 20-second protocols; more than 1 µm for fossil and unannealed induced tracks measured in this study, and 0.7-1.2 µm in Durango apatite measurements in the experimental data sets used for annealing models.

These differences in latent versus measured lengths in unannealed and lightly geologically annealed track populations highlight a potential shortcoming in the etching procedures employed for the past few decades. Few if any such tracks are fully etched, as etching is halted when track revelation is still somewhere in the decelerating zone. This in turn amplifies the consequences of analyst disagreement about etching extent. By stopping etching as soon as the curve of length versus time in step-etch experiments was reached, the community has essentially set up camp on the edge of a cliff. A change in etching procedure to allow tracks at all levels of annealing to etch more completely may be worth considering.

https://doi.org/10.5194/gchron-2020-31
Preprint. Discussion started: 20 October 2020

6.6 Optimizing the etching protocol

The $v_T(x)$ model framework provides a quantitative basis for evaluating whether the etching procedures used today are the most effective at their goal, which is to provide high numbers of reproducible and informative measurements to constrain thermal histories. For example, the model makes clear that the longer we etch, the more tracks we get that fulfill a given tip clarity criterion. As etching continues, fully-etched tracks may become over-etched, though at a rate defined by v_B, which may be obtainable from etch figure measurements parallel and perpendicular to the **c** axis, D_{par} and D_{per} (Tamer and Ketcham, 2020a). For v_B=0.022 µm/s, five extra seconds of etching leads to only a 0.22 µm increase in length for a previously fully-etched track, which is close to the resolution limit of individual track length measurements. Non-fully-etched tracks will lengthen somewhat more, depending on the etching rates toward the tips. However, because the "short side" of the track length distribution is defined by analyst selection criteria, if these criteria are held consistent, the change in mean length will always be diminished. This suggests that over-etching may not be a significant concern, except to the extent that it makes a grain more difficult to measure due to the enlargement of multiple etched features, and that it has the advantage of increasing the number of well-etched confined tracks available.

We test this proposition using the modeling shown in Table 4 and Figure 16 to estimate what occurs with 25 s of etching rather than 20 s, for various track types and selection criteria. Using the same selection criterion (v_T/v_B = 12), mean unannealed track lengths rise by up to just over 0.3 µm, but the number of selectable tracks increases by almost fourfold for the slowest-etching tracks (spontaneous). Standard deviations rise by less than 0.1 µm. One can even become more restrictive with etching criteria (v_T/v_B = 8) and still have more tracks to measure, with a tighter distribution, although a more increased mean length.

The Figure 16 histograms also provide an instructive summary of the evolution of confined versus selected tracks. The slowest-etching population (SE3) has far more short than long tracks after 20 seconds, which starts to level out by 25 seconds as the number of tracks that are closer to fully etched begins to build up. This trend continues for the next slowest etching population (SE1), with long tracks eventually outnumbering shorter ones, which in time will culminate in a near-steady-state distribution like the fastest-etching example (SE4). Although the proportion of selectable annealed induced tracks only increases modestly with the additional etching time, the fact that a thermal treatment may significantly increase etching rates and thus revelation efficiency suggests that a carefully controlled preheating step could greatly increase confined track numbers, potentially without affecting lengths and thus paleothermal information.

Of course, changes in etching protocol cannot be considered from the standpoint of length measurements alone; possible effects on track density measurements also need to be considered.

6.7 Counting efficiency

The semi-track penetration component of the $v_T(x)$ model (Fig. 3A) also provides some insights into track counting efficiency, and thus age determination. Efficiency in this context is the measured track density divided by the true track density, or the proportion of tracks crossing the polished surface that are detected. Jonckheere and Van den Haute (1996) denote efficiency

https://doi.org/10.5194/gchron-2020-31
Preprint. Discussion started: 20 October 2020

with two variables, ηq, to reflect that it contains both geometric (η) and observer (q) components that are difficult to disentangle. Generally, track etching rates relative to bulk etching rates are too high in apatite to apply the geometric critical angle equation of Fleischer and Price (1964), $\delta_c = \sin^{-1}(v_B/v_T)$, where δ_c is the dip below which tracks become undetectable because surface etching is faster than track etching. The implied efficiency, $\eta = 1 - \sin^2\delta_c \approx 1$ for $v_T >> v_B$, is far higher than the generally observed factor of ~0.9. Jonckheere and Van Den Haute (2002) propose instead the concept of a critical depth, z_c, defining the degree of penetration into the polished surface a track must achieve to be observed, distinguished from other features, and counted with confidence by the analyst. They estimate z_c values of 0.8 µm for apatite and 0.5 µm for muscovite detectors in their data, and propose that efficiency may vary with track length in a way that compounds the effect of length in the first-principles fission track age equation.

The $v_T(x)$ model corroborates and extends these conclusions. Figure 17 shows the near-surface portion of the penetration model for fossil and unannealed and annealed induced tracks, and compares penetration after 20 seconds for the three. The rapid falloff in penetration reflects the tracks that originated above the polished surface, and only extend a short distance into the grain below it. The spacing of the one-second contours reflects the mean etching rate of track tips at depth through time; the slower etching unannealed tracks (Fig. 17A, B) penetrate more slowly than the fast-etching annealed tracks (Fig. 17C, D), but eventually all cases converge to closely-spaced contours reflecting bulk etching. The divergence of the 20-second lines reflects a combination of the different mean track lengths and the etching velocities. If we assume a z_c of 0.8 µm, the implied ηq factors are 0.918 for SE1 and SE6 ($\bar{L}$ = 15.8 µm and 15.0 µm, respectively), 0.912 for SE3 ($\bar{L}$ = 14.4 µm), and 0.902 for SE4 ($\bar{L}$ = 12.3 µm). With further annealing the disparity in efficiency will grow, with estimated ηq falling to 0.8 at 7.7 µm mean track length (Jonckheere and Van Den Haute, 2002). Essentially, shorter track lengths are less efficiently counted because a higher proportion of those that cross the polished surface do not penetrate it sufficiently to be detected reliably. This effect is superimposed on the already understood reduction in track density due to shorter tracks being less likely to cross the polished surface in the first place (e.g., Fleischer et al., 1975).

Variable etching rates further affect this picture. The faster etch rates of SE4 and SE6 increase their track detection efficiencies by allowing the tracks to penetrate more deeply. This is why the ηq for SE6 matches SE1 at 0.8 µm despite lengths being shorter, and is even larger than SE1 at shallower depths. Likewise, if rates for SE4 were more comparable to SE1 and SE3, as may be the case for geologically annealed tracks, the discrepancy in penetration between them, and thus ηq, would be larger. On the other hand, when etching continues after tracks have reached bulk etching rates, as reflected by the closely spaced lines in the latter stages of etching (Fig. 17C,D), shallow etched features may begin to widen and become less distinct, possibly becoming less likely to be recognized as tracks. Deeper penetration might then be required for detection, essentially lowering z_c for faster-etching tracks, which would have a similar effect on efficiency.

In practice, lower counting efficiency for shorter tracks could mean that the ages of older, more annealed grains may be under-estimated because more tracks are missed. Insofar as zeta calibration is based on measurement of standards with low levels of annealing (Durango, Fish Canyon), this effect may make old samples appear younger, leading, for example, to an increased

https://doi.org/10.5194/gchron-2020-31
Preprint. Discussion started: 20 October 2020

possibility of inversion of apatite fission-track and (U-Th)/He ages (e.g., Flowers et al., 2009). It may also affect the way such samples are quantitatively interpreted using thermal history modeling. The currently used relationship between length and density is based on the data and normalizations put forward by Green (1988), and attempts at first principles derivations of this relationship are ground-truthed against those data (e.g., Ketcham, 2003). If, for example, geological annealing results in different etching rates than laboratory annealing, the laboratory-measured relation may be biased.

Finally, we note the relatively steep slopes of the depth versus penetration curves (Fig. 17E), which correspond to about 1% efficiency (0.01 relative penetration) per 0.1 μm depth, assuming the z_c model is correct. This highlights the critical role of consistency in mount preparation and polishing, and short semi-track identification, in achieving reproducible ages.

6.7 Outlook

Although the $v_T(x)$ model provides a range of insights into the fission track revelation and measurement process, these results should be only viewed as preliminary, and far more data are required to construct a complete picture that can fully inform practical apatite fission track analysis. Detailed step-etching measurements of fossil tracks at various stages of natural annealing, and induced tracks at more advanced stages of annealing, are required to fill out our database of how etching velocities evolve, including the advent of unetchable gaps. We particularly note that apatites have a range of solubilities, which will affect both etching rates and tip appearances and thus selection biases; work on apatites beyond Durango is thus a necessity. In addition, the effects of track **c**-axis angle need to be incorporated into the modeling, which would be aided by larger step-etching data sets better documenting a range of angles.

Such efforts can be combined with further community-level work to verify the extent to which analytical procedure and analyst criteria are responsible for the disappointing lack of consistency in fission-track length data between research groups. If v_T/v_B or something like it can be established as the primary driver of divergence, it will empower the community to make its data both more reproducible and more plentiful. It is likely that etching procedures can be optimized to provide more abundant confined tracks, while creating an improved, quantitative link to the experimental data sets that underlie annealing models. Follow-on rewards will also include quantitative linkages between experimental data sets across laboratory groups, etching protocols, and even apatite varieties, as well as a more complete picture of track structure, all of which will improve our understanding of annealing.

Ultimately, as image capture, storage, and processing become more commonplace and more powerful, the possibility of using image analysis to evaluate the degree of track etching will grow. Development of the requisite capabilities promises to not only make length data more consistent, but also more information-rich by characterizing etching extent, and thus true underlying latent length, on an individual track level.

https://doi.org/10.5194/gchron-2020-31
Preprint. Discussion started: 20 October 2020

7 Conclusions

A new, comprehensive model of confined fission track etching successfully fits a range of detailed step-etching data for Durango apatite, and illuminates details of track structure and the nature of the measurement process. Specific findings include:

- Along-track etching velocity, $v_T(x)$, varies within and among fission tracks, and affects all length measurements as executed with current protocols.
- Fission tracks that have only experienced relatively low, near-Earth-surface temperatures etch more slowly than tracks that have been subjected to high temperatures in the laboratory (≥ 235°C, 24 h).
- For many track populations, especially at low levels of annealing, only a small proportion of tracks that are intersected are seen and selected for measurement. Etching extent and analyst decision-making are more influential than length biasing in determining which track populations are more likely to be measured, which in turn affects the fidelity of thermal history modeling using track lengths.
- The fall-off in track etching velocity toward track tips, and variability among analysts in how they judge fission tracks to be sufficiently etched for measurement, is likely to be the major factor underlying poor reproducibility. Most variation in a major inter-laboratory measurement experiment can be explained by varying only the threshold for track selection, characterized as the ratio of along-track and bulk etching velocities at the etched track tip (v_T/v_B).
- A normalization procedure that accounts for analyst decision-making (e.g., v_T/v_B), in the context of an overall etching model, will be more robust than one based on mean track length measurements alone.
- The $v_T(x)$ model has the potential to allow optimization of etching protocols to maximize both confined track yield and information content, while retaining a quantitative link to the experimental annealing data sets that underlie thermal history modeling.
- Variable along-track etch rates may also influence the efficiency of semi-track counting for age determinations, and our understanding of the length-density relationship that underlies thermal history modeling.

https://doi.org/10.5194/gchron-2020-31
Preprint. Discussion started: 20 October 2020

Appendix: $v_T(x)$ Etching Model Equations

We characterize the latent track as a set of etching rates along the track central axis, *x*, with the starting point for etching, or point where the impinging etchant pathway intersects the latent track, denoted as x_{int}. In the Constant-core model, the track middle section is assumed have to a constant etching rate v_{Tmax} over length extent Δx_{Tmax}, beyond which etching rate falls at linear rate *A* over distance $\Delta x_{T_{max}-B}$ until it drops by $\Delta v_{T_{max}-B}$ to v_B. In the Linear model, $\Delta x_{T_{max}-B} = 0$. Defining our coordinate system such that the track extends in the positive direction from one tip at *x*=0, we define coordinates x_{B_1} and x_{B_2} to be the track tips, beyond which etching occurs at the bulk rate; and x_{T_1} and x_{T_2} demarking the central zone of maximum track etch rate (see Figure 1):

$$v_T(x) = \begin{cases} v_{T_{max}} & x_{T_1} \le x \le x_{T_2} \quad \text{(A1a)} \\ v_{Tmax} - A\left|x - x_{T_1 \text{ or } T_2}\right|;\ A = \left|\dfrac{\Delta v_{T_{max}-B}}{\Delta x_{T_{max}-B}}\right| & x_{B_1} \le x < x_{T_1};\ x_{T_2} < x \le x_{B_2} \quad \text{(A1b)} \\ v_B & x < x_{B_1};\ x_{B_2} < x \quad \text{(A1c)} \end{cases}$$

The full latent length is

$$L_{lat} = \Delta x_{Tmax} + 2\Delta x_{T_{max}-B} \quad \text{(A2)}$$

We next derive the time required to etch a confined half-track starting at point x_{int} and going toward one end. To begin, we etch in the positive direction toward x_{B_2}, and denote the etched half-length L_2. Etching of the grain mount commences at time *t*=0, and the confined track starts to etch at a later time t_s, to account for the time necessary to etch the impinging track and then widen it sufficiently to intersect the confined track. We back-step though the three possible zones where etching may begin. If x_{int} is in the right-hand zone between x_{T_2} and x_{B_2}, then the time required to etch to a half-length L_2 is

https://doi.org/10.5194/gchron-2020-31
Preprint. Discussion started: 20 October 2020

$$t(L_2) = \begin{cases} t_s + \int_{x_{int}}^{x_{int}+L_2} \frac{dx}{v_T(x)} & L_2 \le x_{B_2} - x_{int} \quad \text{(A3a)} \\ t_s + \int_{x_{int}}^{x_{B2}} \frac{dx}{v_T(x)} + \frac{L_2 - (x_{B_2} - x_{int})}{v_B} & x_{B_2} - x_{int} < L_2 \quad \text{(A3b)} \end{cases}$$

Expanding the integral term:

$$\int \frac{dx}{v_T(x)} = \int \frac{dx}{[v_{T_{max}} - A(x - x_{T_2})]} = \frac{1}{A}\int \frac{dx}{v_{T_{max}}/A + x_{T_2} - x} = \frac{-1}{A}\ln\left(\frac{v_{T_{max}}}{A} + x_{T_2} - x\right) \quad \text{(A4)}$$

using

$$\frac{-1}{A}\int \frac{du}{u} = \frac{-1}{A}\ln(u)\ with\ u = a - x; a = \frac{v_{T_{max}}}{A} + x_{T_2}; du = -dx$$

leads to the solution:

$$t(L_2) = \begin{cases} t_s - \frac{1}{A}\ln\left(1 - \frac{L_2}{\frac{v_{T_{max}}}{A} + x_{T_2} - x_{int}}\right) & L_2 \le x_{B_2} - x_{int} \quad \text{(A5a)} \\ t_s - \frac{1}{A}\ln\left(\frac{\frac{v_{T_{max}}}{A} + x_{T_2} - x_{B_2}}{\frac{v_{T_{max}}}{A} + x_{T_2} - x_{int}}\right) + \frac{L_2 - (x_{B2} - x_{int})}{v_B} & x_{B_2} - x_{int} < L_2 \quad \text{(A5b)} \end{cases}$$

https://doi.org/10.5194/gchron-2020-31
Preprint. Discussion started: 20 October 2020

If x_{int} is in the central zone with maximum etching rate, then:

$$t_s + \frac{L_2}{v_{T_{max}}} \qquad L_2 \le x_{T_2} - x_{int} \tag{A6a}$$

$$t(L_2) = \quad t_s + \frac{x_{T_2} - x_{int}}{v_{T_{max}}} + \int_{x_{T_2}}^{x_{int}+L_2} \frac{dx}{v_T(x)} \qquad x_{T_2} - x_{int} < L_2 \le x_{B_2} - x_{int} \tag{A6b}$$

$$t_s + \frac{x_{T_2} - x_{int}}{v_{T_{max}}} + \int_{x_{T_2}}^{x_{B2}} \frac{dx}{v_T(x)} + \frac{L_2 - \left(x_{B_2} - x_{int}\right)}{v_B} \qquad x_{B_2} - x_{int} < L_2 \tag{A6c}$$

After integrating, the solution becomes:

$$t_s + \frac{L_2}{v_{T_{max}}} \qquad L_2 \le x_{T_2} - x_{int} \tag{A7a}$$

$$t(L_2) = \quad t_s + \frac{x_{T_2} - x_{int}}{v_{T_{max}}} - \frac{1}{A}\ln\left(1 + \frac{x_{T_2} - (x_{int} + L_2)}{\frac{v_{T_{max}}}{A}}\right) \qquad x_{T_2} - x_{int} < L_2 \le x_{B_2} - x_{int} \tag{A7b}$$

$$t_s + \frac{x_{T_2} - x_{int}}{v_{T_{max}}} - \frac{1}{A}\ln\frac{v_B}{v_{T_{max}}} + \frac{L_2 - \left(x_{B_2} - x_{int}\right)}{v_B} \qquad x_{B_2} - x_{int} < L_2 \tag{A7c}$$

600

https://doi.org/10.5194/gchron-2020-31
Preprint. Discussion started: 20 October 2020

Finally, if x_{int} is in the left-hand zone between x_{T_1} and x_{B_1}:

$$t_s + \int_{x_{int}}^{x_{int}+L_2} \frac{dx}{v_T(x)} \qquad L_2 \le x_{T_1} - x_{int} \tag{A8a}$$

$$t_s + \int_{x_{int}}^{x_{T_1}} \frac{dx}{v_T(x)} + \frac{L_2 - (x_{T_1} - x_{int})}{v_{T_{max}}} \qquad x_{T_1} - x_{int} < L_2 \le x_{T_2} - x_{int} \tag{A8b}$$

$$t(L_2) = \begin{cases} t_s + \int_{x_{int}}^{x_{T_1}} \frac{dx}{v_T(x)} + \frac{x_{T_2} - x_{T_1}}{v_{T_{max}}} + \int_{x_{T_2}}^{x_{int}+L_2} \frac{dx}{v_T(x)} & x_{T_2} - x_{int} < L_2 \le x_{B_2} - x_{int} \quad \text{(A8c)} \\ t_s + \int_{x_{int}}^{x_{T_1}} \frac{dx}{v_T(x)} + \frac{x_{T_2} - x_{T_1}}{v_{T_{max}}} + \int_{x_{T_2}}^{x_{B_2}} \frac{dx}{v_T(x)} + \frac{L_2 - (x_{B_2} - x_{int})}{v_B} & x_{B_2} - x_{int} < L_2 \quad \text{(A8d)} \end{cases}$$

Integrating leads to:

$$t_s + \frac{1}{A}\ln\left(1 + \frac{L_2}{\frac{v_{T_{max}}}{A} + x_{int} - x_{T_1}}\right) \qquad L_2 \le x_{T_1} - x_{int} \tag{A9a}$$

$$t_s - \frac{1}{A}\ln\left[1 + \frac{A(x_{int} - x_{T_1})}{v_{T_{max}}}\right] + \frac{L_2 - (x_{T_1} - x_{int})}{v_{T_{max}}} \qquad x_{T_1} - x_{int} < L_2 \le x_{T_2} - x_{int} \tag{A9b}$$

$$t(L_2) = \begin{cases} t_s - \frac{1}{A}\ln\left[1 + \frac{A(x_{int} - x_{T_1})}{v_{T_{max}}}\right] + \frac{x_{T_2} - x_{T_1}}{v_{T_{max}}} - \frac{1}{A}\ln\left(1 + \frac{A(x_{T_2} - x_{int} - L_2)}{v_{T_{max}}}\right) & x_{T_2} - x_{int} < L_2 \le x_{B_2} - x_{int} \quad \text{(A9c)} \\ t_s - \frac{1}{A}\ln\left[1 + \frac{A(x_{int} - x_{T_1})}{v_{T_{max}}}\right] + \frac{x_{T_2} - x_{T_1}}{v_{T_{max}}} - \frac{1}{A}\ln\frac{v_B}{v_{T_{max}}} + \frac{L_2 - (x_{B_2} - x_{int})}{v_B} & x_{B_2} - x_{int} < L_2 \quad \text{(A9d)} \end{cases}$$

https://doi.org/10.5194/gchron-2020-31
Preprint. Discussion started: 20 October 2020

Solving each set of equations for length as a function of etching time, and transforming the length boundaries to time boundaries, in the right-hand zone:

$$0 \qquad t \le t_s \tag{A10a}$$

$$L_2(t) = \begin{cases} \left(\frac{v_{T_{max}}}{A} + x_{T_2} - x_{int}\right)\left[1 - e^{-A(t-t_s)}\right] & t_s < t \le t_s + \frac{1}{A}\ln\left(\frac{v_{T_{max}} + A\left(x_{T_2} - x_{int}\right)}{v_B}\right) \quad \text{(A10b)} \\ v_B\left[t - t_s - \frac{1}{A}\ln\left(\frac{v_{T_{max}} + A\left(x_{T_2} - x_{int}\right)}{v_B}\right)\right] + \left(x_{B2} - x_{int}\right) & t_s + \frac{1}{A}\ln\left(\frac{v_{T_{max}} + A\left(x_{T_2} - x_{int}\right)}{v_B}\right) < t \quad \text{(A10c)} \end{cases}$$

In the central zone:

$$0 \qquad t \le t_s \tag{A11a}$$

$$v_{T_{max}}(t - t_s) \qquad t_s < t \le t_s + \frac{x_{T_2} - x_{int}}{v_{T_{max}}} \tag{A11b}$$

$$L_2(t) = \begin{cases} x_{T_2} - x_{int} + \frac{v_{T_{max}}}{A}\left[1 - e^{-A\left(t - t_s - \frac{x_{T_2} - x_{int}}{v_{T_{max}}}\right)}\right] & t_s + \frac{x_{T_2} - x_{int}}{v_{T_{max}}} < t \le t_s + \frac{x_{T_2} - x_{int}}{v_{T_{max}}} - \frac{1}{A}ln\left(\frac{v_B}{v_{T_{max}}}\right) \quad \text{(A11c)} \\ x_{B_2} - x_{int} + v_B\left[t - t_s - \frac{x_{T_2} - x_{int}}{v_{T_{max}}} + \frac{1}{A}ln\left(\frac{v_B}{v_{T_{max}}}\right)\right] & t_s + \frac{x_{T_2} - x_{int}}{v_{T_{max}}} - \frac{1}{A}ln\left(\frac{v_B}{v_{T_{max}}}\right) < t \quad \text{(A11d)} \end{cases}$$

https://doi.org/10.5194/gchron-2020-31
Preprint. Discussion started: 20 October 2020

GEOCHRONOLOGY Discussions Open Access EGU

610 And in the left-hand zone:

$$0 \qquad t \le t_s \tag{A12a}$$

$$\left(\frac{v_{T_{max}}}{A} + x_{int} - x_{T_1}\right)\left[e^{A(t-t_s)} - 1\right] \qquad t_s < t \le t_s - \frac{1}{A}\ln\left[1 + \frac{A\left(x_{int} - x_{T_1}\right)}{v_{T_{max}}}\right] \tag{A12b}$$

$$L_2(t) = \begin{cases} x_{T_1} - x_{int} + v_{T_{max}}\left\{t - t_s + \frac{1}{A}\ln\left[1 + \frac{A\left(x_{int} - x_{T_1}\right)}{v_{T_{max}}}\right]\right\} & t_s - \frac{1}{A}\ln\left[1 + \frac{A\left(x_{int} - x_{T_1}\right)}{v_{T_{max}}}\right] < t \le t_s - \frac{1}{A}\ln\left[1 + \frac{A\left(x_{int} - x_{T_1}\right)}{v_{T_{max}}}\right] + \frac{x_{T_2} - x_{T_1}}{v_{T_{max}}} \\ x_{T_2} - x_{int} - \frac{v_{T_{max}}}{A}\left(e^{-A\left\{t - t_s + \frac{1}{A}\ln\left[1 + \frac{A\left(x_{int} - x_{T_1}\right)}{v_{T_{max}}}\right] - \frac{x_{T_2} - x_{T_1}}{v_{T_{max}}}\right\}} - 1\right) & t_s - \frac{1}{A}\ln\left[1 + \frac{A\left(x_{int} - x_{T_1}\right)}{v_{T_{max}}}\right] + \frac{x_{T_2} - x_{T_1}}{v_{T_{max}}} < t \le t_s - \frac{1}{A}\ln\left[1 + \frac{A\left(x_{int} - x_{T_1}\right)}{v_{T_{max}}}\right] + \frac{x_{T_2} - x_{T_1}}{v_{T_{max}}} - \frac{1}{A}\ln\frac{v_B}{v_{T_{max}}} \\ x_{B_2} - x_{int} + v_B\left\{t - t_s + \frac{1}{A}\ln\left[1 + \frac{A\left(x_{int} - x_{T_1}\right)}{v_{T_{max}}}\right] - \frac{x_{T_2} - x_{T_1}}{v_{T_{max}}} + \frac{1}{A}\ln\frac{v_B}{v_{T_{max}}}\right\} & t_s - \frac{1}{A}\ln\left[1 + \frac{A\left(x_{int} - x_{T_1}\right)}{v_{T_{max}}}\right] + \frac{x_{T_2} - x_{T_1}}{v_{T_{max}}} - \frac{1}{A}\ln\frac{v_B}{v_{T_{max}}} < t \end{cases} \tag{A12c, A12d, A12e}$$

To solve for the other half-length, L_1, we use the same set of equations and simply change the value of x_{int} to $L_{lat} - x_{int}$.

https://doi.org/10.5194/gchron-2020-31
Preprint. Discussion started: 20 October 2020

Code Availability

The modelling introduced in this contribution was coded in the IDL programming language. The GitHub repository containing the IDL code used to generate our results can be accessed at https://doi.org/10.5281/zenodo.4064290. It is made available under the GPL-3.0 License.

Data Availability

The data are available as an Excel spreadsheet in the Texas Data Repository, at https://doi.org/10.18738/T8/MPWDZI.

Author Contributions

RAK derived and coded the model, interpreted the results, wrote the text, and drafted the figures. MTT planned and executed the measurements and aided with interpretation. RAK and MTT jointly initiated the study, which is an extension of the research program begun with MTTs dissertation.

Competing Interests

The authors declare that they have no competing interests.

Acknowledgements

This work was supported by the Geology Foundation of the Jackson School of Geosciences.

https://doi.org/10.5194/gchron-2020-31
Preprint. Discussion started: 20 October 2020

References

Aslanian, C., Jonckheere, R., Wauschkuhn, B., and Ratschbacher, L.: A quantitative description of fission-track etching in apatite, Am. Mineral., in press.

Barbarand, J., Carter, A., Wood, I., and Hurford, A. J.: Compositional and structural control of fission-track annealing in apatite, Chem. Geol., 198, 107-137, 10.1016/S0009-2541(02)00424-2, 2003.

Carlson, W. D., Donelick, R. A., and Ketcham, R. A.: Variability of apatite fission-track annealing kinetics I: Experimental results, Am. Mineral., 84, 1213-1223, 10.2138/am-1999-0901, 1999.

Dakowski, M.: Length distributions of fission tracks in thick crystals, Nucl. Tracks, 2, 181-189, 10.1016/0145-224X(78)90022-4, 1978.

Donelick, R. A., Ketcham, R. A., and Carlson, W. D.: Variability of apatite fission-track annealing kinetics II: Crystallographic orientation effects, Am. Mineral., 84, 1224-1234, 10.2138/am-1999-0902, 1999.

Fleischer, R. L., and Price, P. B.: Glass dating by fission fragment tracks, J. Geophys. Res., 69, 331-339, 1964.

Fleischer, R. L., Price, P. B., and Woods, R. T.: Nuclear-particle-track identification in inorganic solids, Physical Review, 188, 563-568, 10.1103/PhysRev.188.563, 1969.

Fleischer, R. L., Price, P. B., and Walker, R. M.: Nuclear tracks in solids; principles and applications, Univ. Calif. Press : Berkeley, Calif., United States, United States, 1975.

Flowers, R. M., Ketcham, R. A., Shuster, D. L., and Farley, K. A.: Apatite (U-Th)/He thermochronometry using a radiation damage accumulation and annealing model, Geochim. Cosmochim. Acta, 73, 2347-2365, 2009.

Galbraith, R. F., and Laslett, G. M.: Some calculations relevant to thermal annealing of fission tracks in apatite, Proc. R. Soc. Lond. A, 419, 305-321, 10.1098/rspa.1988.0109, 1988.

Galbraith, R. F., Laslett, G. M., Green, P. F., and Duddy, I. R.: Apatite fission track analysis: geological thermal history analysis based on a three-dimensional random process of linear radiation damage, Phil. Trans. R. Soc. Lond. A, 332, 419-438, 10.1098/rsta.1990.0124, 1990.

Gleadow, A. J. W., Gleadow, S. J., Belton, D. X., Kohn, B. P., Krochmal, M. S., and Brown, R. W.: Coincidence mapping - a key strategy for the automatic counting of fission tracks in natural minerals, Geological Society, London, Special Publications, 324, 25-36, 10.1144/SP324.2, 2009.

Green, P. F., Duddy, I. R., Gleadow, A. J. W., Tingate, P. R., and Laslett, G. M.: Thermal annealing of fission tracks in apatite 1. A qualitative description, Chem. Geol., 59, 237-253, 10.1016/0168-9622(86)90074-6, 1986.

Green, P. F.: The relationship between track shortening and fission track age reduction in apatite: Combined influences of inherent instability, annealing anisotropy, length bias and system calibration, Earth Planet. Sci. Lett., 89, 335-352, 10.1016/0012-821X(88)90121-5, 1988.

Green, P. F., Duddy, I. R., Laslett, G. M., Hegarty, K. A., Gleadow, A. J. W., and Lovering, J. F.: Thermal annealing of fission tracks in apatite 4. Quantitative modeling techniques and extension to geological time scales, Chem. Geol., 79, 155-182, 1989.

https://doi.org/10.5194/gchron-2020-31
Preprint. Discussion started: 20 October 2020

Hurford, A. J.: An Historical Perspective on Fission-Track Thermochronology, in: Fission-Track Thermochronology and its Application to Geology, edited by: Malusa, M. G., and Fitzgerald, P. G., Springer, 3-23, 2019.

Jonckheere, R., and Van Den Haute, P.: Observations on the geometry of etched fission tracks in apatite: Implications for models of track revelation, Am. Mineral., 81, 1476-1493, 1996.

Jonckheere, R., and Van Den Haute, P.: On the frequency distributions per unit area of the projected and etchable lengths of surface-intersecting fission tracks: influences of track revelation, observation and measurement, Rad. Meas., 30, 155-179, 10.1016/S1350-4487(99)00038-4, 1999.

Jonckheere, R., and Van Den Haute, P.: On the efficiency of fission-track counts in an internal and external apatite surface and in a muscovite external detector, Rad. Meas., 35, 29-40, 2002.

Jonckheere, R., Enkelmann, E., Min, M., Trautmann, C., and Ratschbacher, L.: Confined fission tracks in ion-irradiated and step-etched prismatic sections of Durango apatite, Chem. Geol., 242, 202-217, 10.1016/j.chemgeo.2007.03.015, 2007.

Jonckheere, R., Tamer, M. T., Wauschkuhn, B., Wauschkuhn, F., and Ratschbacher, L.: Single-track length measurements of step-etched fission tracks in Durango apatite: "Vorsprung durch Technik", Am. Mineral., 102, 10.2138/am-2017-5988, 2017.

Jonckheere, R., Wauschkuhn, B., and Ratschbacher, L.: On growth and form of etched fission tracks in apatite: A kinetic approach, Am. Mineral., 104, 569-579, 10.2138/am-2019-6762, 2019.

Ketcham, R. A., Donelick, R. A., and Carlson, W. D.: Variability of apatite fission-track annealing kinetics III: Extrapolation to geological time scales, Am. Mineral., 84, 1235-1255, 10.2138/am-1999-0903, 1999.

Ketcham, R. A.: Observations on the relationship between crystallographic orientation and biasing in apatite fission-track measurements, Am. Mineral., 88, 817-829, 10.2138/am-2003-5-610, 2003.

Ketcham, R. A.: Forward and inverse modeling of low-temperature thermochronometry data, in: Low-Temperature Thermochronology, edited by: Reiners, P. W., and Ehlers, T. A., Reviews in Mineralogy and Geochemistry, 58, Mineralogical Society of America, Chantilly, VA, 275-314, 2005.

Ketcham, R. A., Carter, A. C., Donelick, R. A., Barbarand, J., and Hurford, A. J.: Improved modeling of fission-track annealing in apatite, Am. Mineral., 92, 799-810, 10.2138/am.2007.2281, 2007a.

Ketcham, R. A., Carter, A. C., Donelick, R. A., Barbarand, J., and Hurford, A. J.: Improved measurement of fission-track annealing in apatite using c-axis projection, Am. Mineral., 92, 789-798, 10.2138/am.2007.2280, 2007b.

Ketcham, R. A., Guenthner, W. R., and Reiners, P. W.: Geometric analysis of radiation damage connectivity in zircon, and its implications for helium diffusion, Am. Mineral., 98, 350-360, 10.2138/am.2013.4249, 2013.

Ketcham, R. A., Carter, A., and Hurford, A. J.: Inter-laboratory comparison of fission track confined length and etch figure measurements in apatite, Am. Mineral., 100, 1452-1468, 10.2138/am-2015-5167, 2015.

Ketcham, R. A., Van Der Beek, P. A., Barbarand, J., Bernet, M., and Gautheron, C.: Reproducibility of thermal history reconstruction from apatite fission-track and (U-Th)/He data, Geochem. Geophys. Geosys., 19, 10.1029/2018GC007555, 2018.

https://doi.org/10.5194/gchron-2020-31
Preprint. Discussion started: 20 October 2020

Lal, D., Rajan, R. S., and Tamhane, A. S.: Chemical composition of nuclei of Z>22 in cosmic rays using meteoric minerals as detectors, Nature, 221, 33-37, 1969.

Laslett, G. M., Kendall, W. S., Gleadow, A. J. W., and Duddy, I. R.: Bias in measurement of fission-track length distributions, Nucl. Tracks, 6, 79-85, 1982.

Laslett, G. M., Gleadow, A. J. W., and Duddy, I. R.: The relationship between fission track length and track density in apatite, Nucl. Tracks, 9, 29-38, 10.1016/0735-245X(84)90019-X, 1984.

Li, W., Wang, L., Sun, K., Lang, M., Trautmann, C., and Ewing, R. C.: Porous fission fragment tracks in fluorapatite, Phys. Rev. B, 82, 144109, 10.1103/PhysRevB.82.144109, 2010.

Li, W., Lang, M., Gleadow, A. J. W., Zdorvets, M. V., and Ewing, R. C.: Thermal annealing of unetched fission tracks in apatite, Earth Planet. Sci. Lett., 321-322, 121-127, 10.1016/j.epsl.2012.01.008, 2012.

Parker, P., and Cowan, R.: Some properties of line segment processes, J. Appl. Prob., 13, 255-266, 1976.

Paul, T. A., and Fitzgerald, P. G.: Transmission electron microscopic investigation of fission tracks in fluorapatite, Am. Mineral., 77, 336-344, 1992.

Press, W. H., Flannery, B. P., Teukolsky, S. A., and Vettering, W. T.: Numerical Recipes in C, Cambridge University Press, Cambridge, 735 pp., 1988.

Tagami, T., and O'Sullivan, P. B.: Fundamentals of fission-track thermochronology, in: Low-Temperature Thermochronology, edited by: Reiners, P. W., and Ehlers, T. A., Reviews in Mineralogy and Geochemistry, 58, Mineralogical Society of America, Chantilly, VA, 19-47, 2005.

Tamer, M. T., Chung, L., Ketcham, R. A., and Gleadow, A. J. W.: Analyst and etching protocol effects on the reproducibility of apatite confined fission-track length measurement, and ambient-temperature annealing at decadal timescales, Am. Mineral., 104, 1421-1435, 10.2138/am-2019-7046, 2019.

Tamer, M. T., and Ketcham, R. A.: Is low-temperature fission-track annealing in apatite a thermally controlled process?, Geochem. Geophys. Geosys., 21, e2019GC008877, 10.1029/2019GC008877, 2020a.

Tamer, M. T., and Ketcham, R. A.: The along-track etching structure of fission tracks in apatite: Observations and implications, Chem. Geol., 553, 119809, 10.1016/j.chemgeo.2020.119809, 2020b.

Wauschkuhn, B., Jonckheere, R., and Ratschbacher, L.: The KTB apatite fission-track profiles: Building on a firm foundation?, Geochim. Cosmochim. Acta, 167, 27-62, j.gca.2015.06.015, 2015a.

Wauschkuhn, B., Jonckheere, R., and Ratschbacher, L.: Xe- and U-tracks in apatite and muscovite near the etching threshold, Nucl. Instr. Meth. Phys. Res. B, 343, 146-152, 10.1016/j.nimb.2014.11.072, 2015b.

Willett, S. D.: Inverse modeling of annealing of fission tracks in apatite 1: A controlled random search method, Am. J. Sci., 297, 939-969, 1997.

Table 1: Data and model fits

			Measured						Constant-core model					Linear model				
Fission tracks	Exp.[1]	Etch Time (s)	*N*	l_m (µm)	dl_m (µm)	σ (µm)	z_{znt}[2] (µm)	*Int./ trk.*[3]	l_m (µm)	σ (µm)	*%sel*[4]	t_s[5] (s)	z_{int}[2] (µm)	l_m (µm)	σ (µm)	*%sel*[4]	t_s[5] (s)	z_{int}[2] (µm)
Induced unannealed	SE1	20	72	15.77	0.08	0.67			15.6	0.6	5.0%	7.1	3.0	15.6	0.6	5.3%	7.2	3.1
		25	72	16.35	0.08	0.72			16.6	0.5				16.6	0.5			
		30	72	16.92	0.09	0.77	3.86	1.7	16.9	0.5				17.0	0.5			
	SE2	10	127	9.89	0.18	1.97			10.0	1.5	11%	4.9	2.4	10.0	1.4	12%	4.9	2.5
		20	127	16.19	0.07	0.80			16.2	0.4				16.2	0.4			
		25	127	16.99	0.07	0.82			16.8	0.5				16.9	0.5			
		30	127	17.18	0.08	0.86	4.43	2.5	17.1	0.5				17.1	0.5			
Spontaneous Cf-irradiated	SE3	10	47	9.11	0.30	2.08			8.9	1.4	5.8%	3.9	2.0	9.6	1.3	14%	4.6	2.2
		15	47	13.03	0.28	1.95			13.3	0.8				13.5	0.6			
		20	47	14.89	0.11	0.73			14.9	0.5				15.0	0.4			
		25	47	15.43	0.11	0.76			15.5	0.5				15.5	0.5			
		30	47	15.69	0.11	0.76	2.70	3.5	15.7	0.5				15.8	0.5			
	TK20	20	87	14.43	0.08	0.78			14.4	0.6	4.4%	6.3	2.5	14.3	0.6	8.9%	7.2	2.7
Induced Annealed (280°C, 24h)	SE4	20	146	12.33	0.07	0.87			12.4	0.5	46%	10.7	3.8	12.4	0.5	47%	10.7	3.8
		25	146	12.64	0.07	0.85			12.7	0.5				12.7	0.5			
		30	146	12.93	0.07	0.83	2.81	5.5	12.9	0.5				12.9	0.5			
	EAE1	10	57	11.25	0.12	0.93	1.99	3.4	11.2	0.8	36%	5.4	3.2	11.2	0.8	36%	5.4	3.2
Induced Annealed (270°C, 24h)	SE5	15	113	12.58	0.09	1.00			12.5	1.4	53%	8.9	3.8	12.5	1.1	56%	8.9	3.9
		20	113	13.48	0.09	0.96			13.6	0.5				13.6	0.5			
		25	113	13.87	0.09	0.95			13.8	0.5				13.9	0.5			
		30	113	14.15	0.09	0.95	1.33	5.8	14.1	0.5				14.1	0.5			
	EAE2	10	94	11.76	0.14	1.36	1.50	4.1	11.8	1.5	31%	5.4	3.2	11.9	1.0	36%	5.4	3.3
Induced Annealed (235°C, 24h)	SE6	15	105	13.77	0.13	1.32			13.9	1.2	57%	8.9	4.3	13.9	1.2	57%	8.9	4.3
		20	105	15.13	0.08	0.78			15.1	0.5				15.1	0.5			
		25	105	15.34	0.08	0.79			15.4	0.5				15.4	0.5			
		30	105	15.65	0.08	0.78	1.43	6.3	15.6	0.5				15.6	0.5			
	EAE3	10	81	13.38	0.12	1.12	1.62	4.2	13.3	1.2	36%	5.4	3.7	13.3	1.2	36%	5.4	3.7

[1]Experiment code; SE and EAE measurements from Tamer and Ketcham (2020b); TK20 measurements from Tamer and Ketcham (2020a).
[2]Mean depth of intersection by semi-track (all intersections for measured data, first intersection for models).
[3]Semi-track intersections per track.
[4]Percent of confined tracks that pass selection criteria.
[5]Mean time selected tracks start etching (are intersected by semi-tracks).

https://doi.org/10.5194/gchron-2020-31
Preprint. Discussion started: 20 October 2020

GEOCHRONOLOGY Discussions
Open Access
EGU

https://doi.org/10.5194/gchron-2020-31
Preprint. Discussion started: 20 October 2020

GEOCHRONOLOGY Discussions Open Access EGU

Table 2: Best-fit model parameters, ranges of comparable fits, and goodness of fit

Data	Constant-core model					Linear model				
	v_{Tmax} (µm/s)	Δx_{Tmax} (µm)	L_{lat} (µm)	χ^2_ν	χ^2_ν r.v.[1]	v_{Tmax} (µm/s)	L_{lat} (µm)	χ^2_ν	χ^2_ν r.v.[1]
SE1+SE2	1.334 (1.109 - 1.698)	4.12 (0.01 - 7.06)	16.96 (16.86 - 17.11)	2.74	4.2%	1.696 (1.625 - 1.750)	17.02 (16.98 - 17.11)	2.81	2.7%
SE3+TK20	0.824 (0.746 - 0.860)	8.68 (7.92 - 9.70)	15.46 (15.37 - 15.53)	0.37	11.2%	1.545 (1.481 - 1.622)	15.62 (15.49 - 15.70)	2.06	5.8%
SE4+EAE1	3.357 (2.836 - 3.587)	0.76 (0.00 - 2.88)	12.45 (12.43 - 12.46)	0.29	2.2%	3.587 (3.561 - 3.625)	12.45 (12.44 - 12.46)	0.28	2.1%
SE5+EAE2	1.767 (1.722 - 1.990)	11.35 (8.28 - 12.85)	13.39 (13.31 - 13.50)	0.97	1.6%	3.544 (3.518 - 3.606)	13.59 (13.55 - 13.59)	1.19	3.1%
SE6+EAE3	4.037 (2.500 - 4.068)	0.19 (0.00 - 7.68)	15.10 (15.04 - 15.13)	0.75	6.5%	4.090 (4.027 - 4.159)	15.10 (15.07 - 15.13)	0.74	5.0%

[1]Relative variation in reduced chi-squared over 20 replicate runs.

https://doi.org/10.5194/gchron-2020-31
Preprint. Discussion started: 20 October 2020

Table 3: Constant-core model predictions of induced unannealed fission track length measurements in Durango apatite based on user selection criterion

v_T/v_B	l_m (µm)	σ (µm)	*%sel*	t_s (s)	z_{int} (µm)
40	13.4	1.7	31%	11.1	3.7
30	14.2	1.3	22%	10.1	3.6
20	15.0	0.9	12%	8.8	3.3
16	15.3	0.7	8.6%	8.1	3.2
12	15.6	0.6	4.9%	7.1	3.0
10	15.8	0.6	3.3%	6.6	2.8
8	16.0	0.5	1.9%	5.9	2.7
4	16.3	0.5	0.15%	3.7	2.0
2	16.8	0.5	0.002%	1.4	0.9

Table 4: Predicted changes in confined track length, standard deviation, and selection efficiency with etching time, selection criteria

		v_T/v_B = 12					v_T/v_B = 8					v_T/v_B = 4				
Sample	Etch time (s)	l_m (µm)	σ (µm)	*%sel*	t_s (s)	z_{int} (µm)	l_m (µm)	σ (µm)	*%sel*	t_s (s)	z_{int} (µm)	l_m (µm)	σ (µm)	*%sel*	t_s (s)	z_{int} (µm)
SE1	20	15.6	0.6	4.9%	7.1	3.0	16.0	0.5	1.9%	5.8	2.7	16.3	0.5	0.2%	3.7	2.0
	25	16.0	0.7	13%	10.5	3.6	16.3	0.6	7.6%	9.1	3.4	16.6	0.5	2.2%	6.9	2.9
SE3[1]	20	14.3	0.6	2.2%	6.8	2.3	14.6	0.5	0.8%	5.7	2.0	14.8	0.5	0.1%	3.9	1.5
	25	14.6	0.6	8.2%	10.0	2.9	14.9	0.5	4.7%	8.9	2.7	15.1	0.5	1.4%	7.1	2.3
SE4	20	12.4	0.5	46%	10.7	3.8	12.4	0.5	41%	10.2	3.8	12.5	0.5	32%	9.4	3.7
	25	12.5	0.6	56%	14.1	3.9	12.5	0.5	51%	13.6	3.9	12.6	0.5	44%	12.8	3.9

[1]Model for SE3 does not include Cf-irradiation, making predictions different from Table 1 (TK20).

https://doi.org/10.5194/gchron-2020-31
Preprint. Discussion started: 20 October 2020

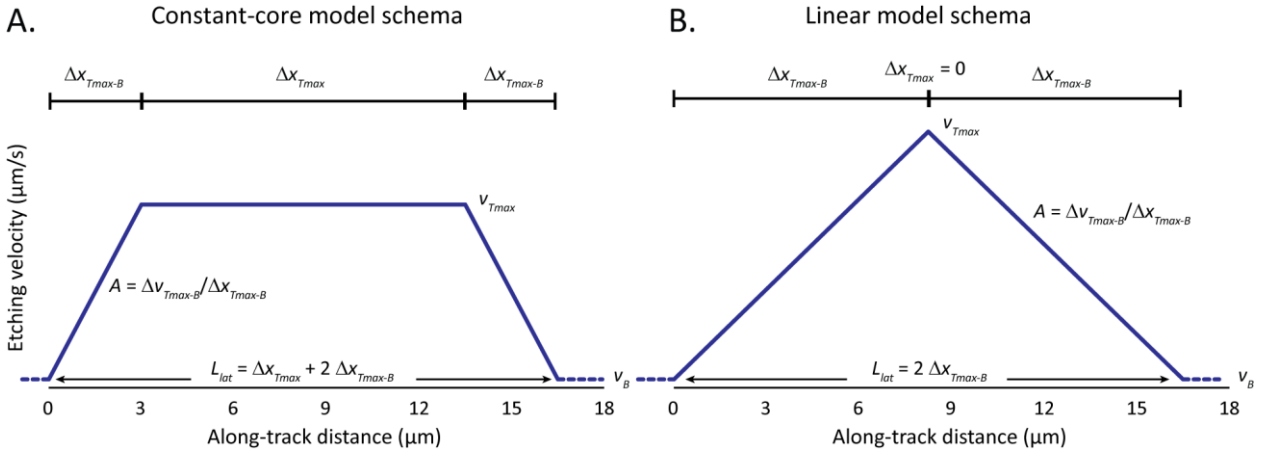

740 **Figure 1: Model schemas for fission-track etching structure. A. Constant-core; B. Linear. v_{Tmax} is maximum along track etching velocity and v_B is bulk grain etching velocity. Δx_{Tmax} is the width of the constant-etching-rate core, and $\Delta x_{Tmax\text{-}B}$ is the width of the zone from the core to the track tip. A is the track etch rate gradient as it falls toward the tip, and L_{lat} is the full latent track length.**

https://doi.org/10.5194/gchron-2020-31
Preprint. Discussion started: 20 October 2020

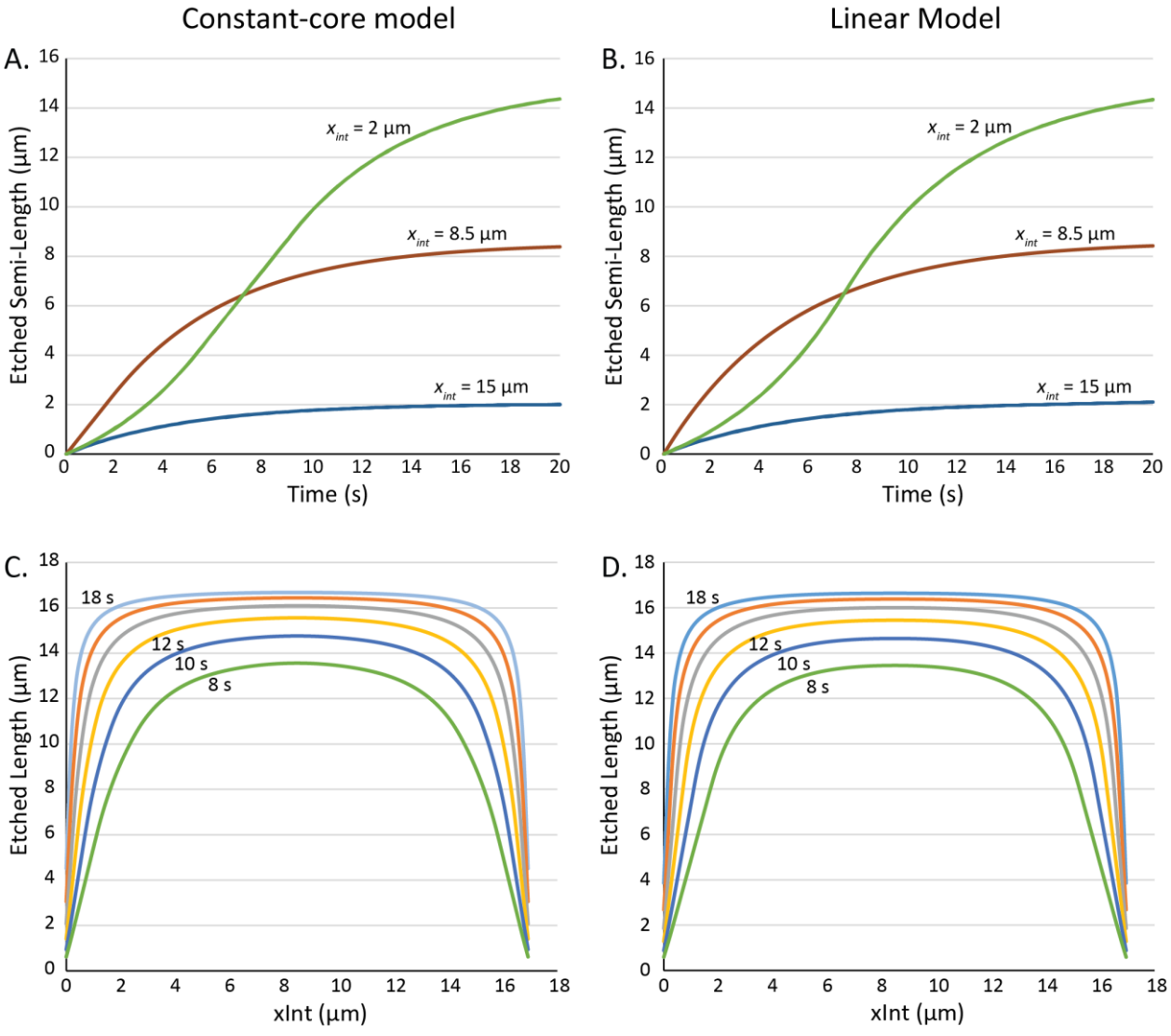

745

Figure 2: Top row: lengthening along unannealed induced fission tracks (latent length 17 µm) starting from midpoint and near each tip, etching from impingement point toward same tip; A. Constant-core model, B. Linear model. Bottom row: evolution of total track length as a function of time, depending on impingement point, at 2-second intervals of total etching time; C. Constant-core model, D. Linear model.

https://doi.org/10.5194/gchron-2020-31
Preprint. Discussion started: 20 October 2020

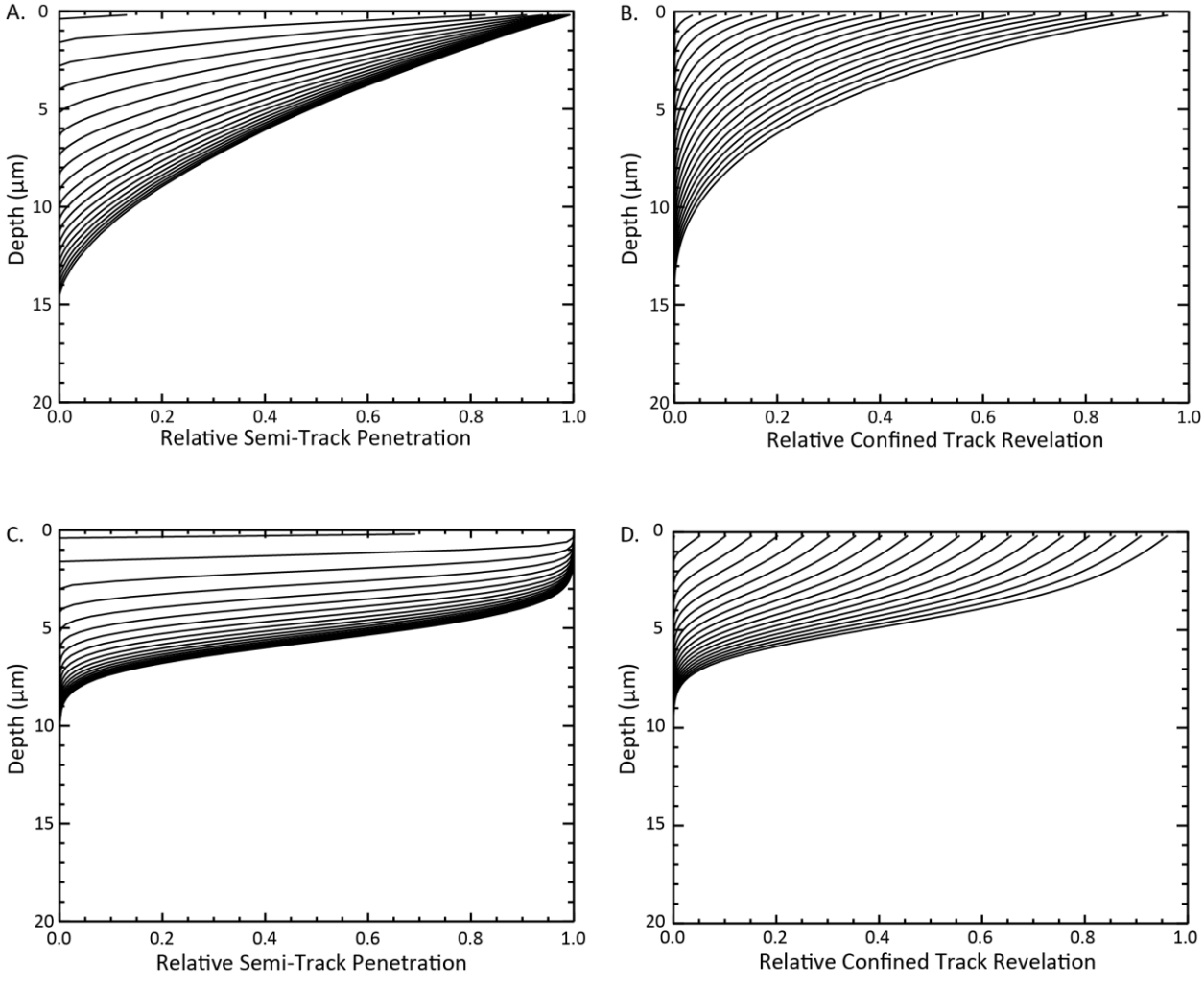

Figure 3: Semi-track penetration and confined track revelation calculated at time steps of 0.2 s and depth steps of 0.2 µm. Lines correspond to relative penetration of semi-tracks and revelation of confined tracks at etching times every second from 1 to 20 s, with the upper left line in each diagram being 1 s and the lower right line being 20s. A, B: Penetration and revelation based on randomly oriented unannealed induced tracks. C, D: Penetration and revelation based on ^{252}Cf tracks oriented at 75° to the grain surface.

https://doi.org/10.5194/gchron-2020-31
Preprint. Discussion started: 20 October 2020

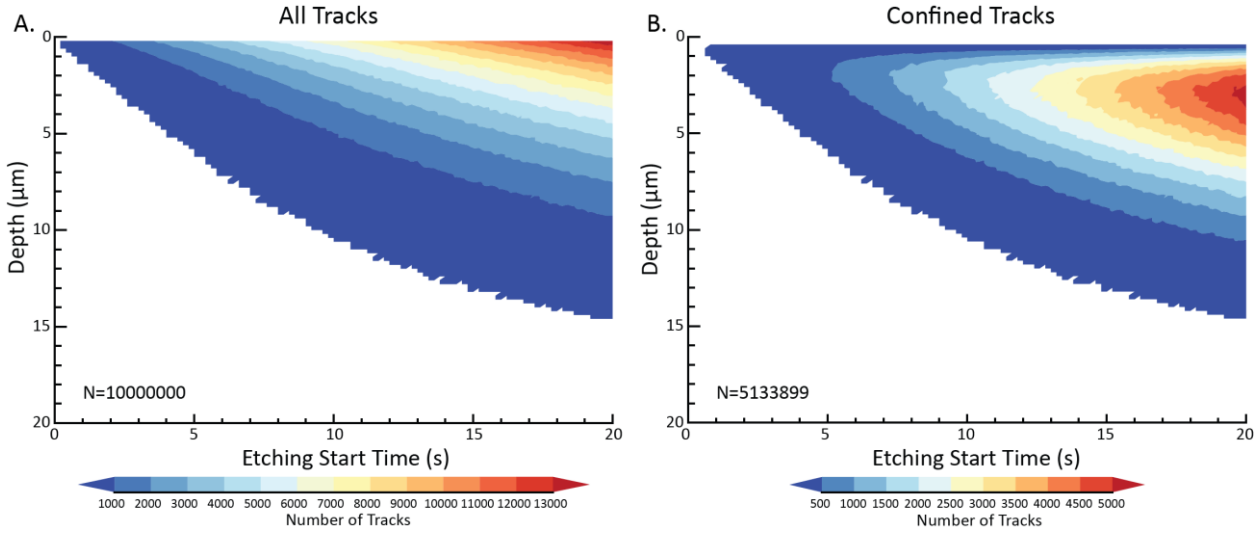

Figure 4: Track intersection results for 10^7 unannealed induced tracks after 20 s of etching. A. Contour diagram of all intersections; B. contour diagram of intersections after excluding tracks that reach the surface (semi-tracks).

https://doi.org/10.5194/gchron-2020-31
Preprint. Discussion started: 20 October 2020

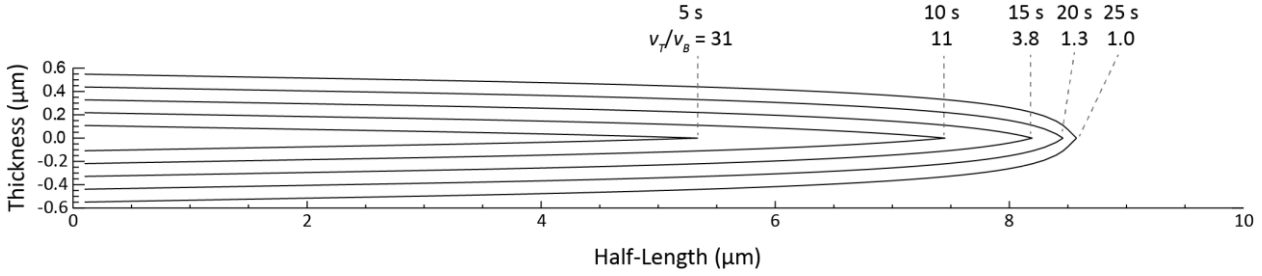

765 **Figure 5: Approximate model of tip evolution and v_T/v_B for constant-core model of an unannealed induced fission track. Each profile starts at the track center, starting from 5 s after the beginning of etching for the innermost profile and proceeding in 5 s increments to 25 s for the outermost profile.**

https://doi.org/10.5194/gchron-2020-31
Preprint. Discussion started: 20 October 2020

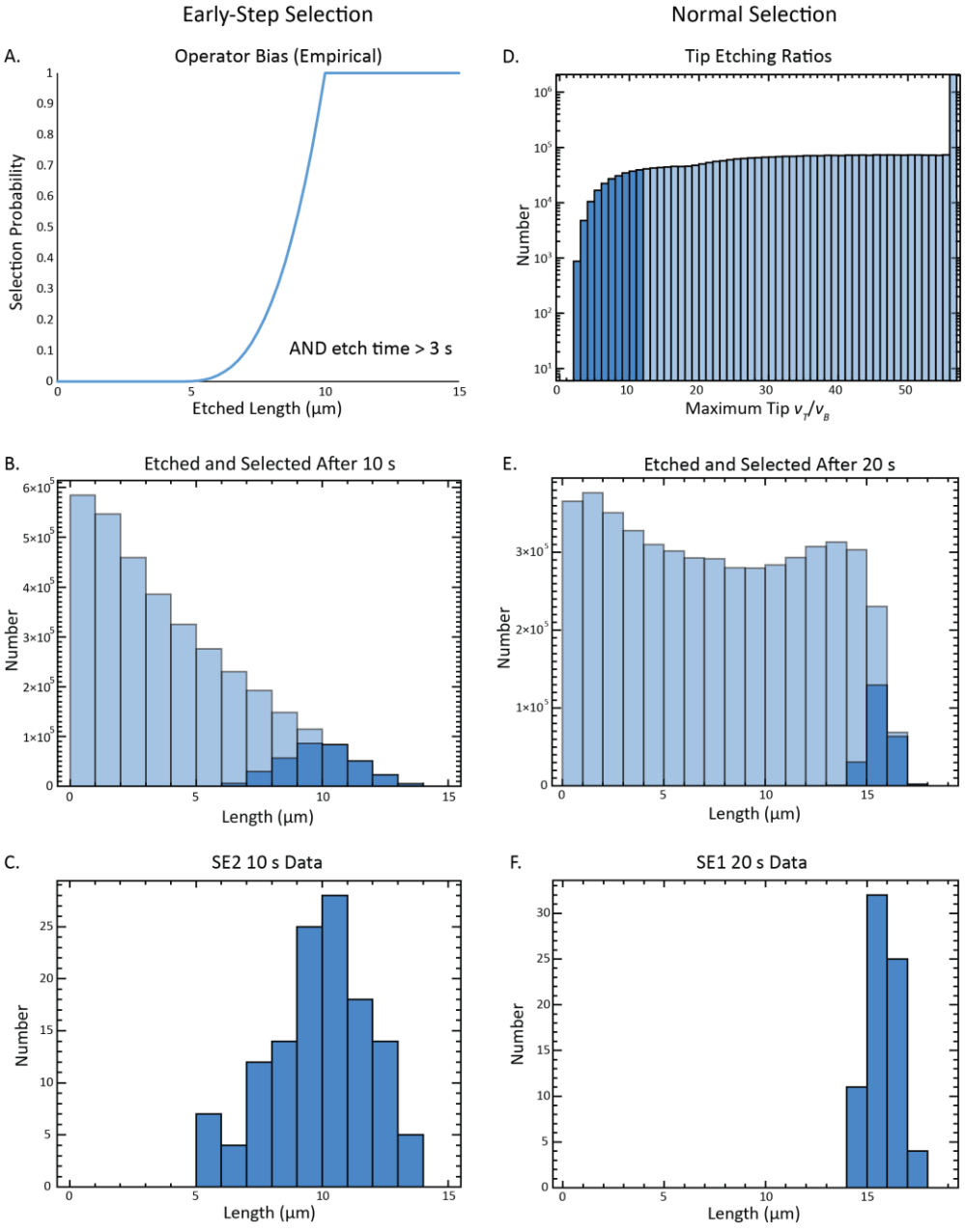

Figure 6: Illustration of how selection criteria for confined fission tracks affects length distributions. In all histograms, faded bars show all etched tracks, and darkened bars show tracks that pass selection criteria. A. Empirical probability function for track selection when first etching step is below 20 s. B. Model histogram for all etched tracks after 10 s (unannealed induced). C. Measured track lengths after 10 s of etching (experiment SE2). D. Model v_T/v_B distribution of unannealed induced tracks after 20 s of etching. E. Model histogram of all etched tracks after 20 s. F. Measured track lengths after a single 20s etch (experiment SE1).

https://doi.org/10.5194/gchron-2020-31
Preprint. Discussion started: 20 October 2020

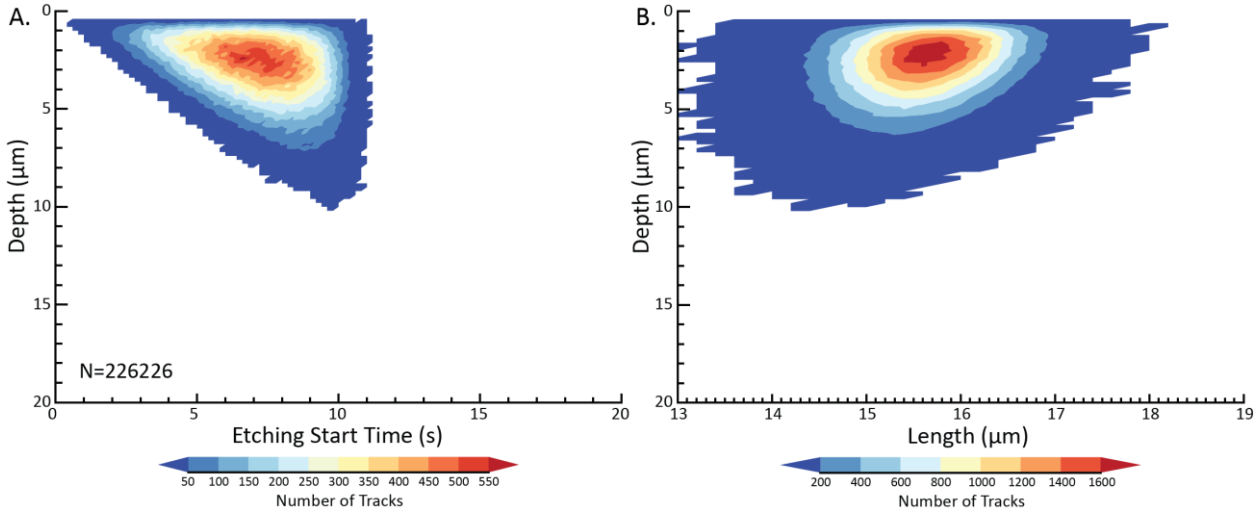

775

Figure 7. Contour diagrams of A. depth vs. length and B. depth vs. etching start time for unannealed induced fission tracks after 20 s of etching.

https://doi.org/10.5194/gchron-2020-31
Preprint. Discussion started: 20 October 2020

780

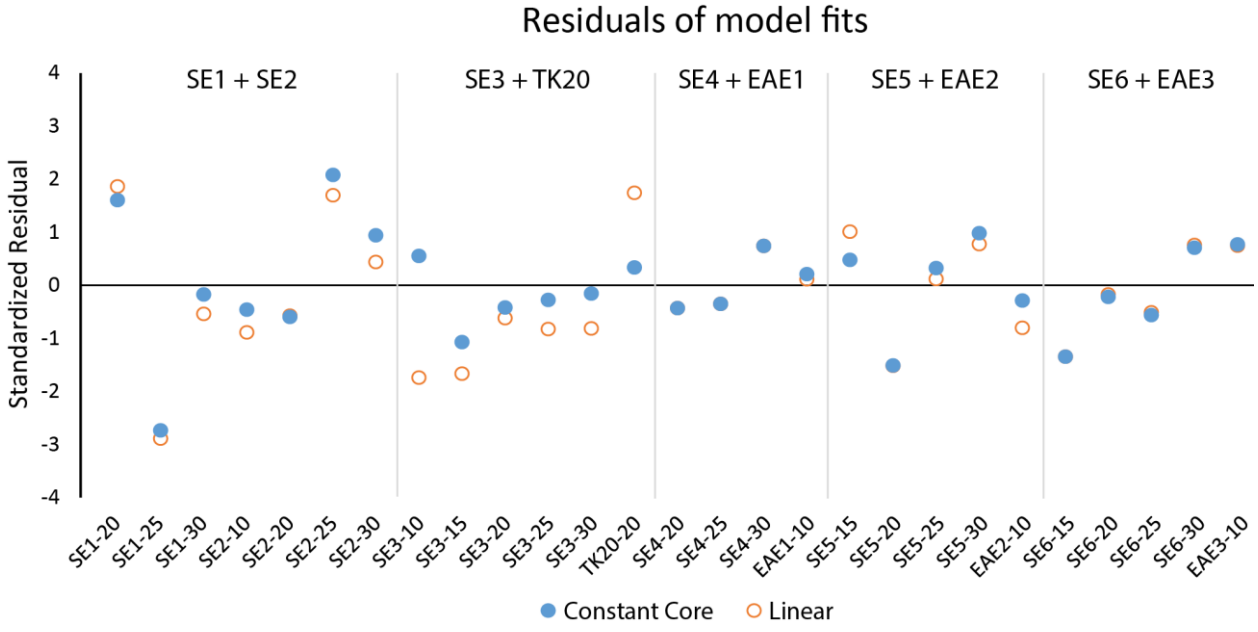

Figure 8: Standardized residuals $(\bar{l} - \bar{l}_{est})/\sigma$ of model fits to each data set.

https://doi.org/10.5194/gchron-2020-31
Preprint. Discussion started: 20 October 2020

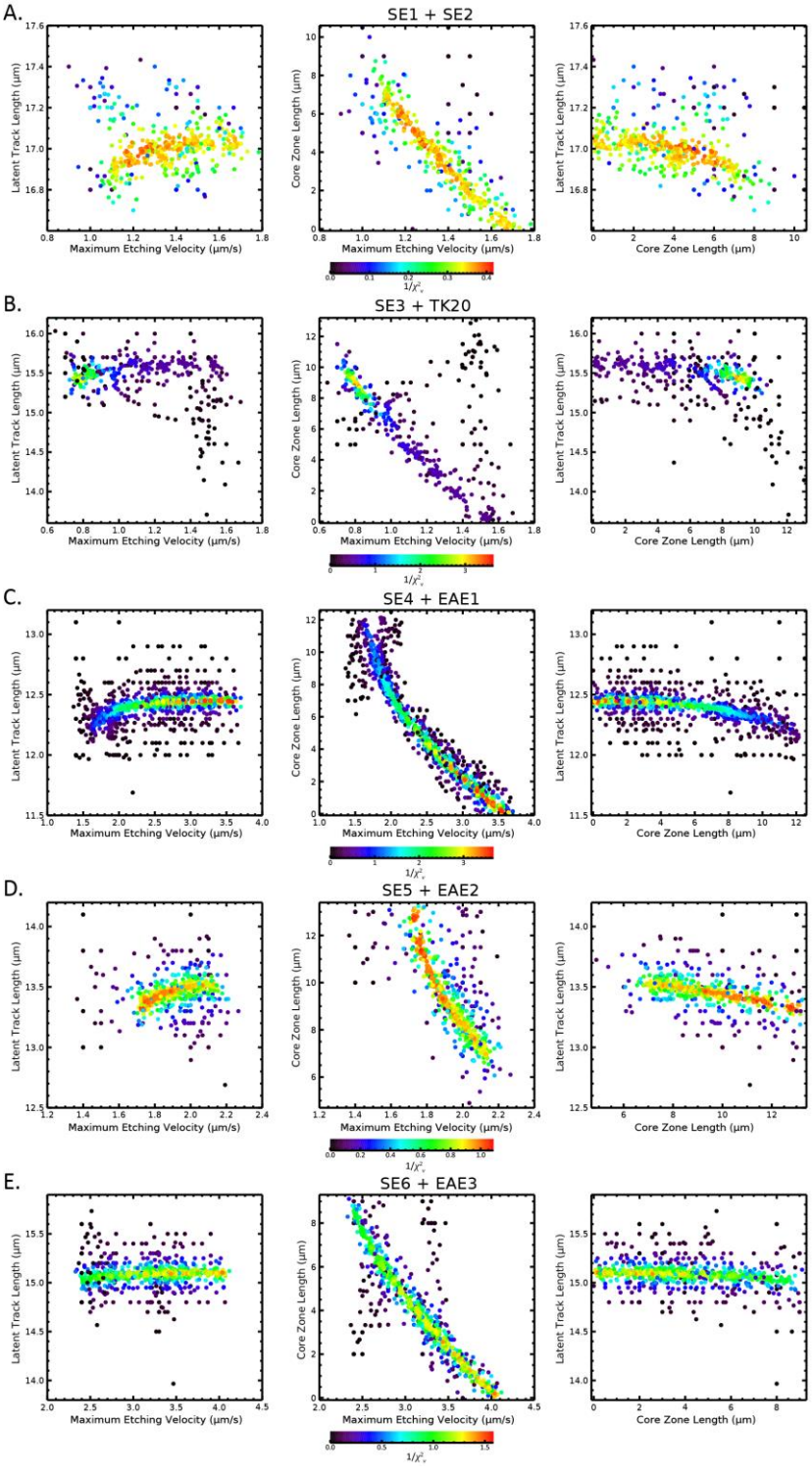

785 **Figure 9: Constant-core model parameter fits**

https://doi.org/10.5194/gchron-2020-31
Preprint. Discussion started: 20 October 2020

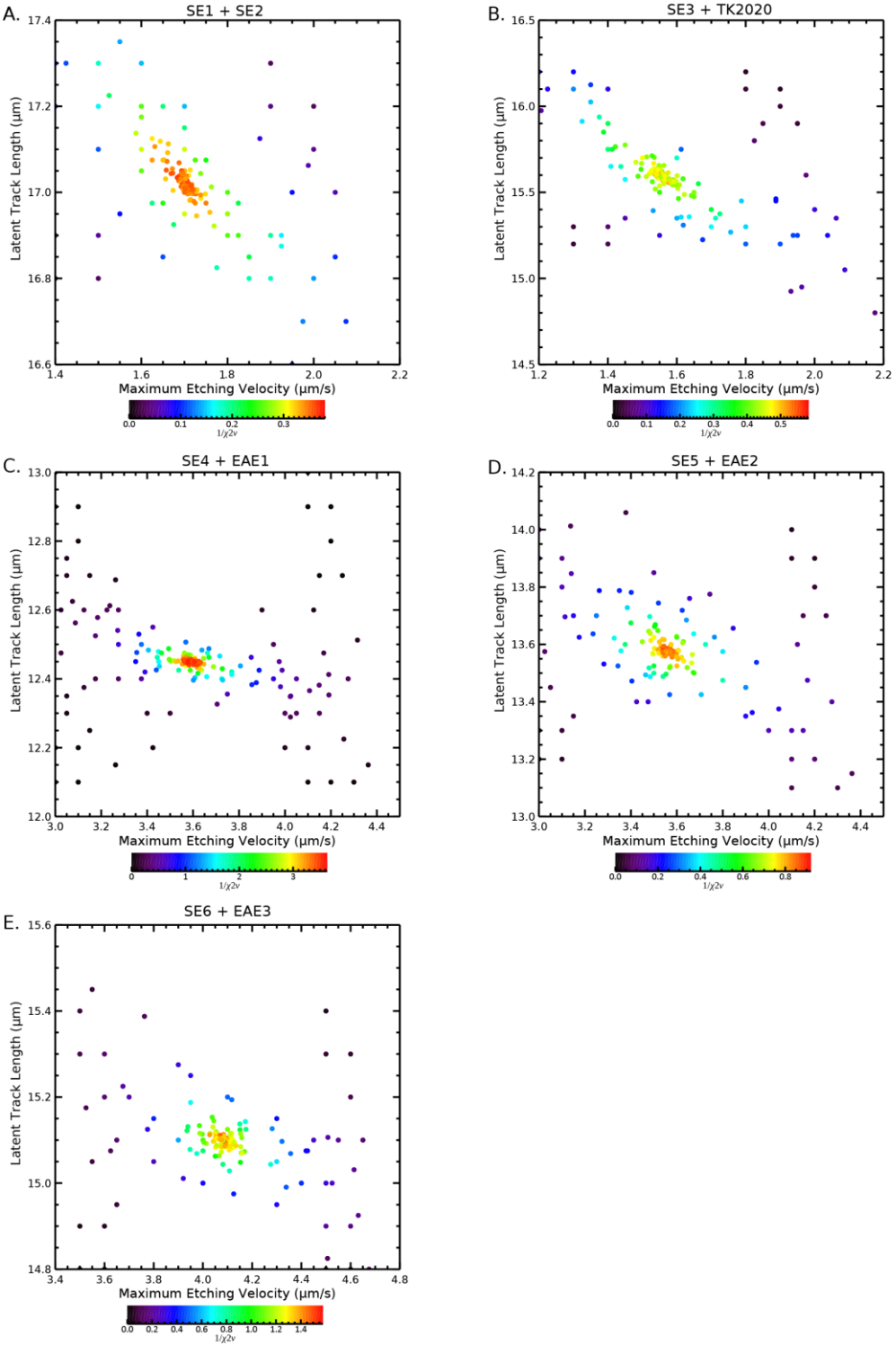

Figure 10: Linear model parameter fits.

https://doi.org/10.5194/gchron-2020-31
Preprint. Discussion started: 20 October 2020

790

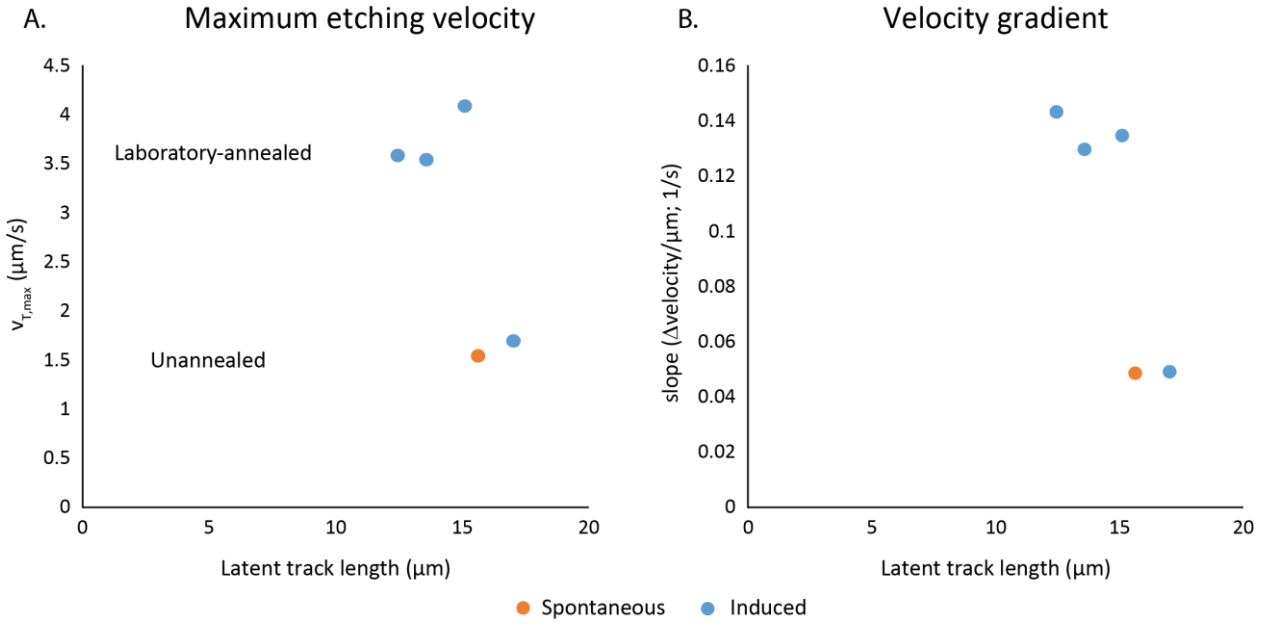

Figure 11: Plots of (A) maximum etching velocity and (B) velocity gradient versus mean latent track length, with high velocities for annealed induced tracks

795

https://doi.org/10.5194/gchron-2020-31
Preprint. Discussion started: 20 October 2020

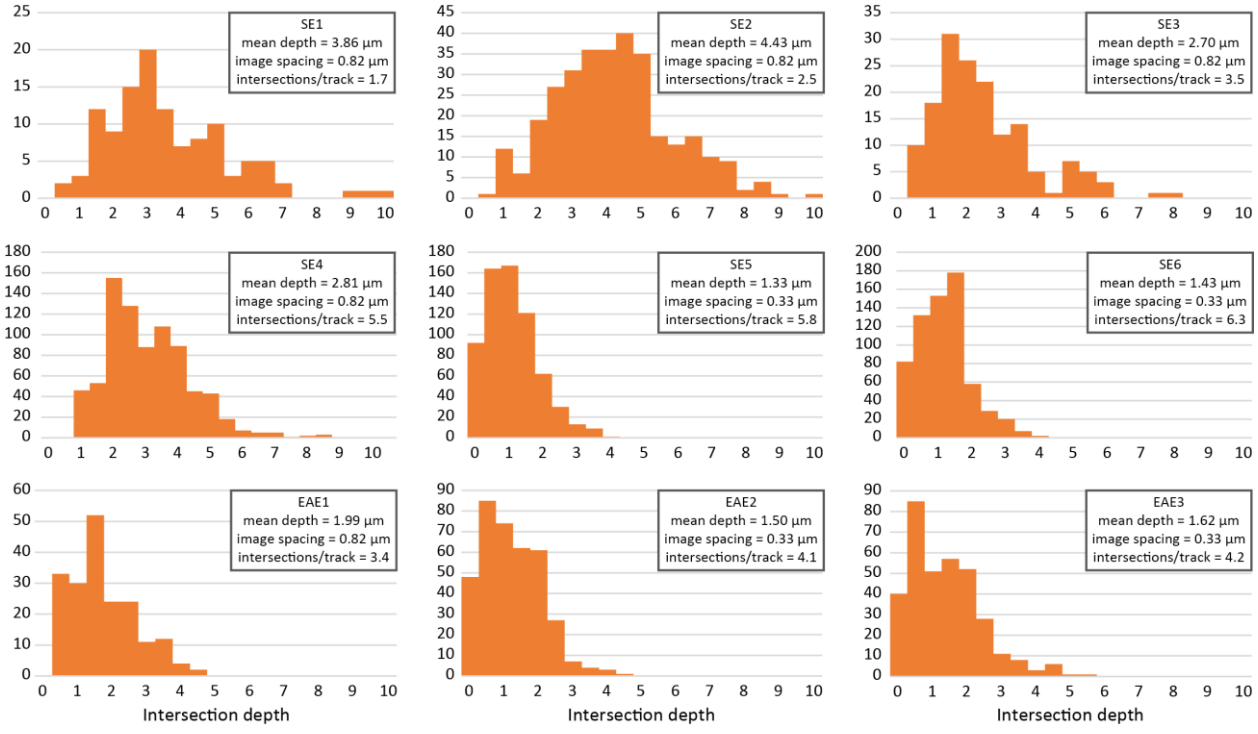

800

Figure 12: Intersection depths of confined tracks for each experiment from Tamer and Ketcham (2020b).

https://doi.org/10.5194/gchron-2020-31
Preprint. Discussion started: 20 October 2020

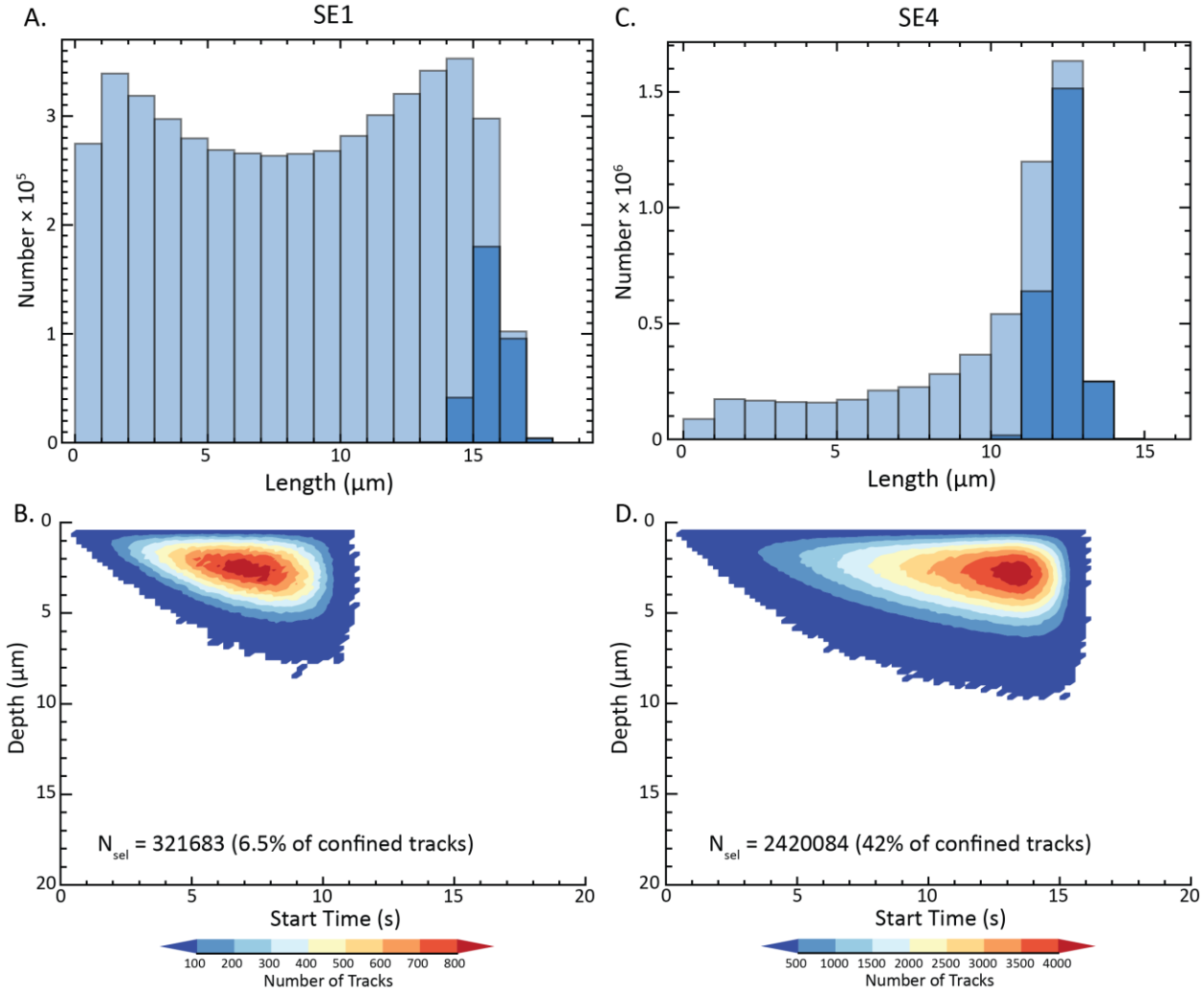

805 **Figure 13: Comparison of the relative efficiency of selecting different track types using a 20-second etching protocol. For unannealed induced tracks (experiment SE1), the great majority of confined tracks intersected have not been etched fully enough to be selected for measurement (A), after they have etched for at least 9 seconds after being intersected (B). Annealed induced tracks (SE4) are both shorter and faster-etching, leading to a much higher proportion of intersected tracks being selectable (C), and shorter required etching times (D).**

810

https://doi.org/10.5194/gchron-2020-31
Preprint. Discussion started: 20 October 2020

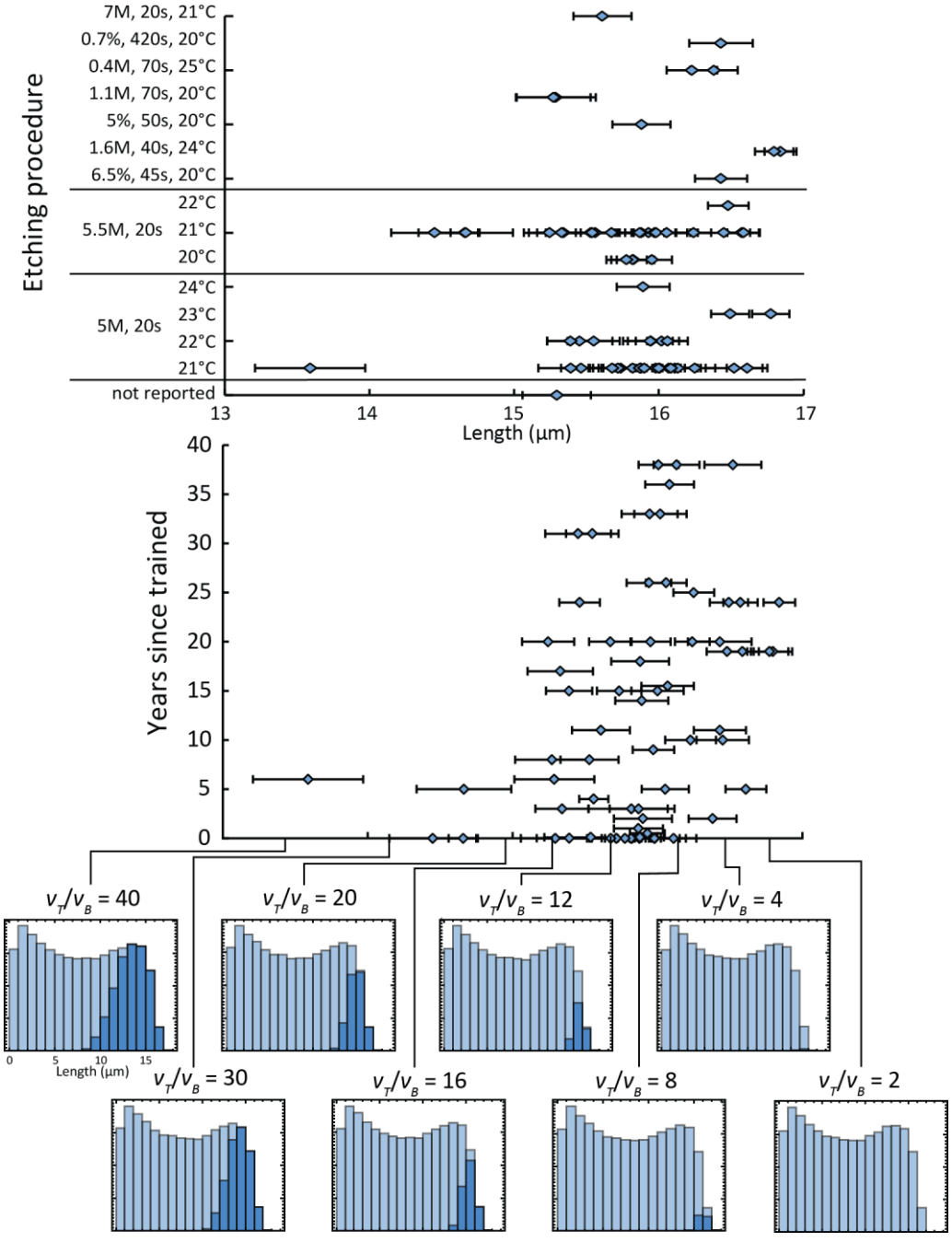

Figure 14: Upper graphs (based on Ketcham et al., 2015; Figure 2C,D) show results of inter-laboratory exercise measuring unannealed induced tracks in Durango apatite, against etching procedure (upper graph) and years since trained in fission-track analysis (middle graph). Histograms below show prediction of Constant-core $v_T(x)$ model, varying only required v_T/v_B for track selection; light bars are unselected tracks, dark bars are selected tracks.

https://doi.org/10.5194/gchron-2020-31
Preprint. Discussion started: 20 October 2020

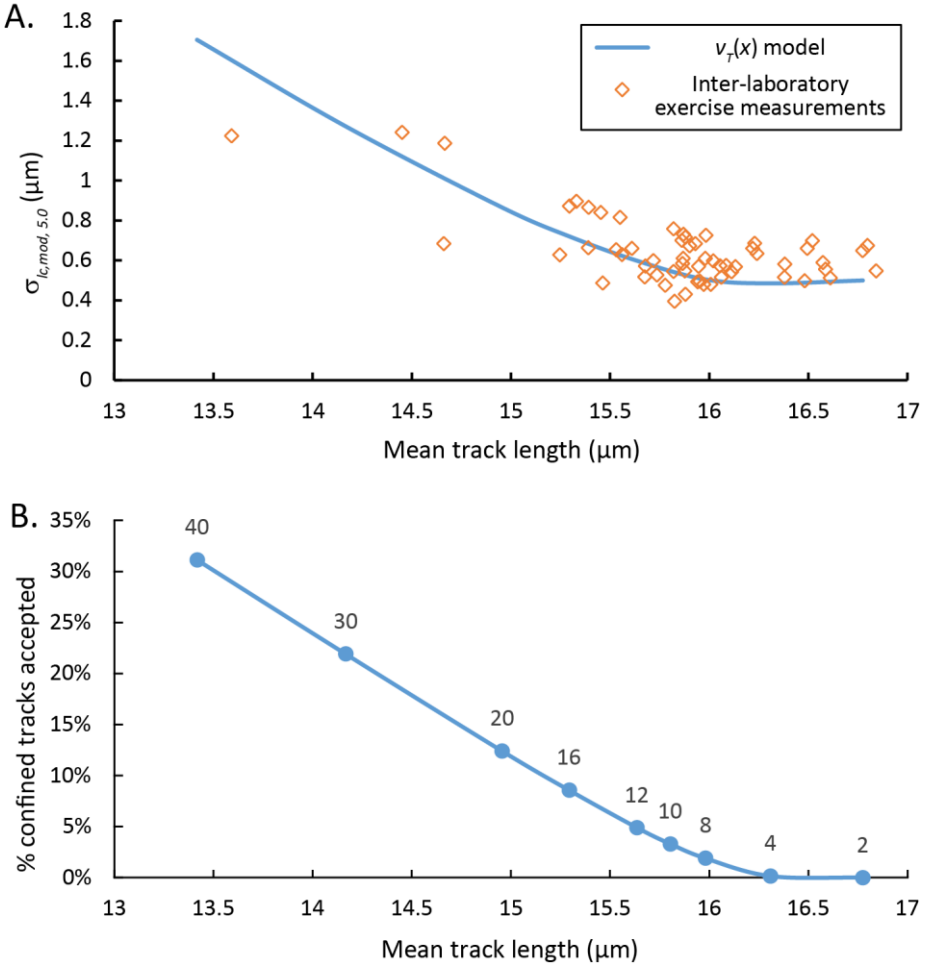

Figure 15: Model relationship between analyst selection criteria (approximated as v_T/v_B at the track tips) and dispersion and efficiency for unannealed induced tracks in Durango apatite. A. Points show the relationship between mean track lengths and standard deviation of c-axis projected lengths, to represent length dispersion without anisotropy effects, from Ketcham et al. (2015) inter-laboratory study. Line shows prediction of $v_T(x)$ model assuming only variation in v_T/v_B, and a baseline 0.5 µm standard deviation of latent track length. B. Curve of efficiency (percent of all confined tracks intersected that are accepted) versus mean track length as it varies with v_T/v_B (values above points).

https://doi.org/10.5194/gchron-2020-31
Preprint. Discussion started: 20 October 2020

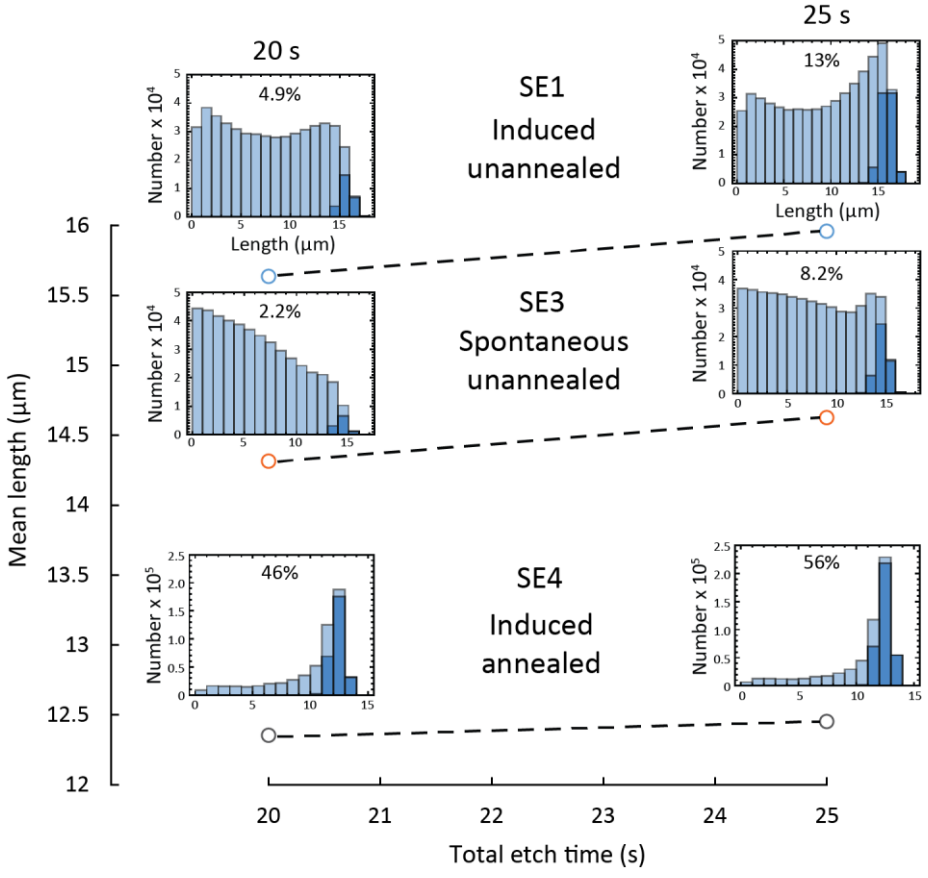

Figure 16: Model predictions of effects of etching for 25 versus 20 seconds, for various track types, assuming selection criterion v_T/v_B = 12. Histograms show confined and selected tracks for each point, and percentages reflect proportion of confined tracks selected. (Note that SE3 model predictions do not presume Cf-irradiation, reducing efficiency compared to Table 1.)

https://doi.org/10.5194/gchron-2020-31
Preprint. Discussion started: 20 October 2020

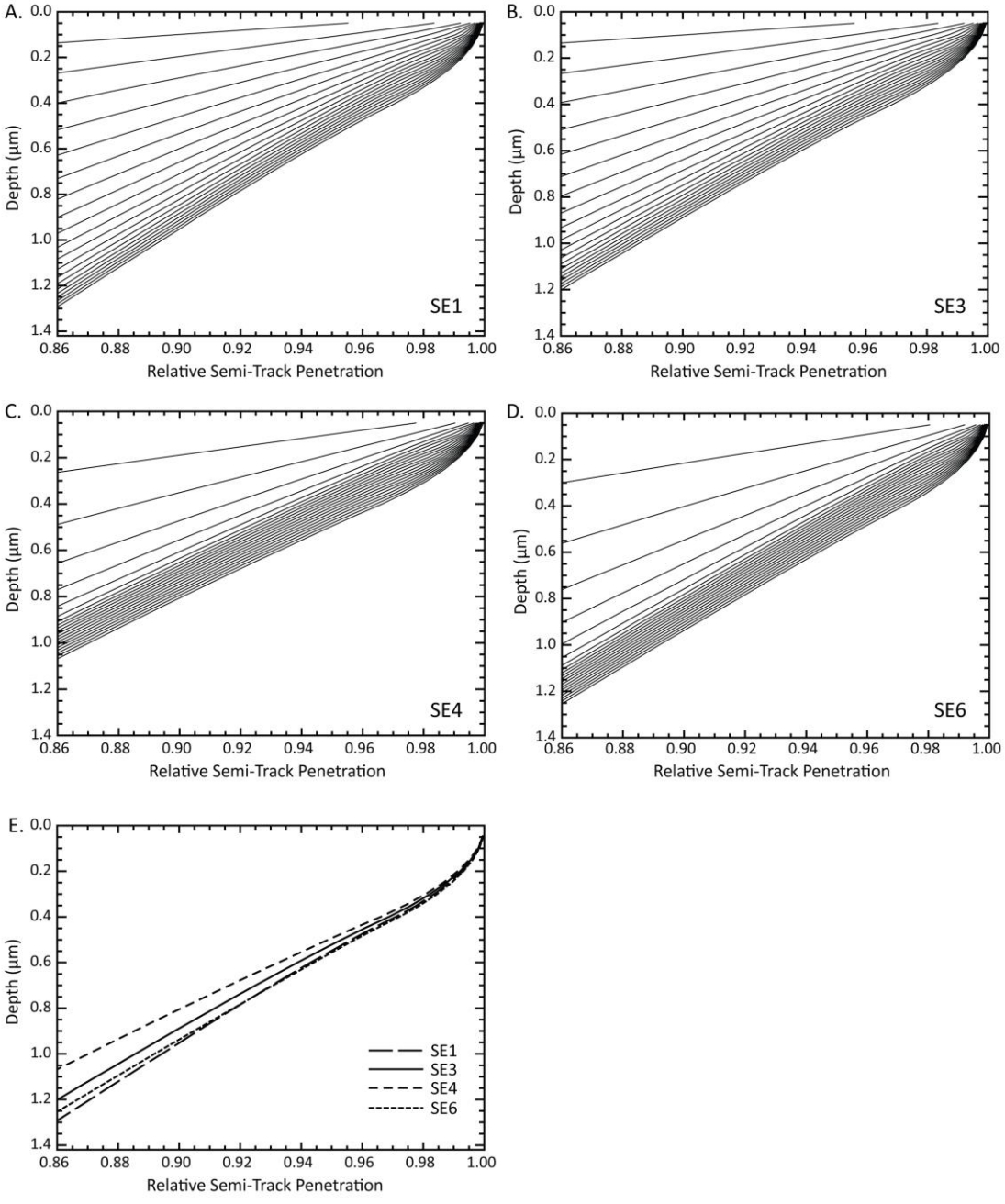

Figure 17: Penetration of semi-tracks near the grain surface, for various track types: A. SE1 Unannealed induced; B. SE3 Unannealed fossil; C. SE4 Annealed induced (280°C, 24h); D. SE6 Annealed Induced (235°C, 24h). In A-D, each line represent penetration in 1-second increments from upper left to bottom right, from 1 to 20 seconds after etching begins. E. 20-second lines for each model.